The University of Texas at Dallas
Center for Quantum Electronics
The Gamma-Ray Laser Project
Quarterly Report
January-March 1989

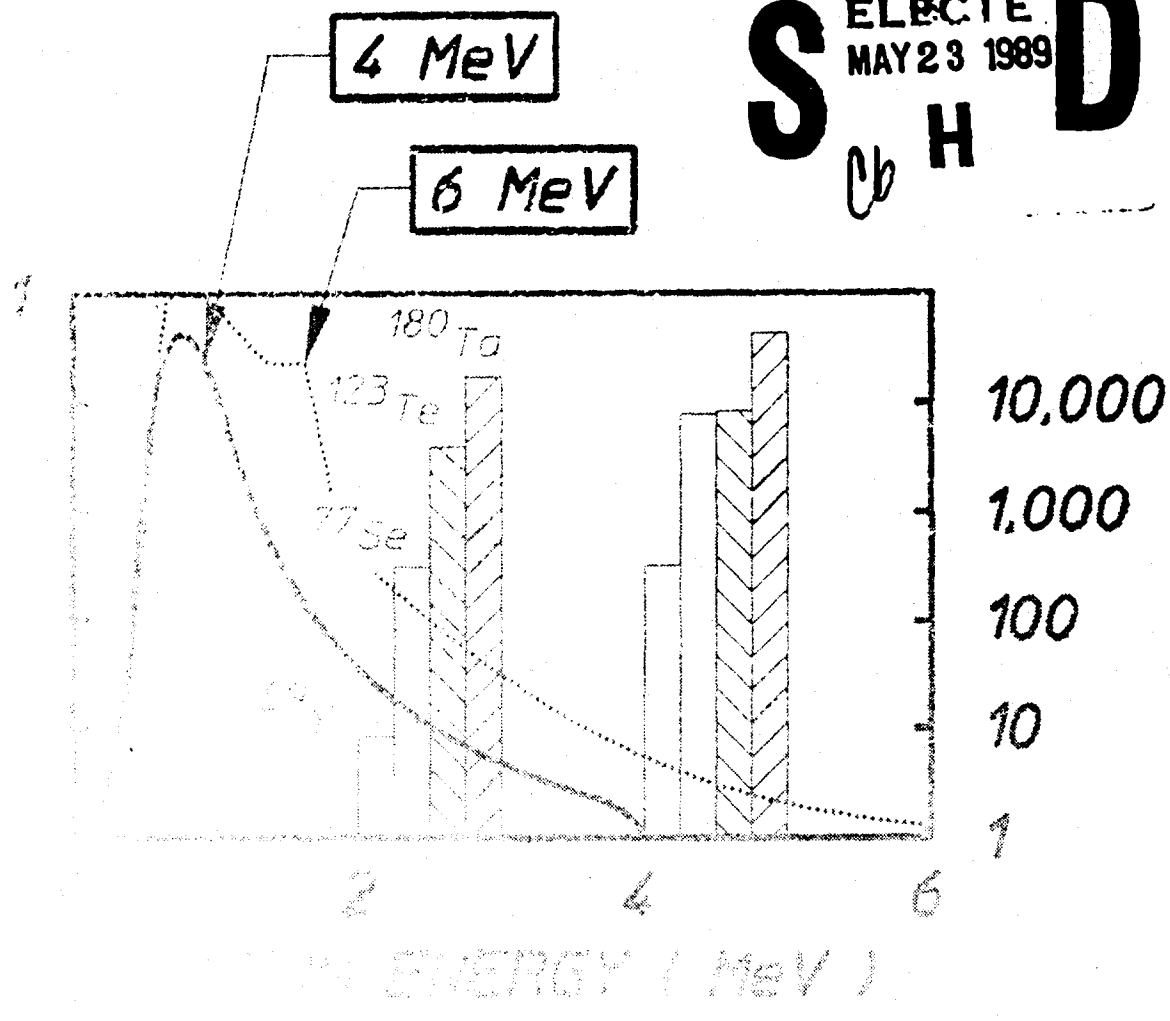

Below 4 MeV, for
$^{180}Ta^{m}(\gamma,\gamma')^{180}Ta$
$\sigma\Gamma = 16000 \times 10^{-29}\ cm^2 keV$

Report GRL/8804

PROOF OF THE FEASIBILITY OF COHERENT AND INCOHERENT SCHEMES FOR PUMPING A GAMMA-RAY LASER

Principal Investigator: Carl B. Collins
The University of Texas at Dallas
Center for Quantum Electronics
P.O. Box 830688
Richardson, Texas 75083-0688

April 1989

Quarterly Technical Progress Report
1 January 1989 through 31 March 1989
Contract Number N00014-86-C-2488

Prepared for
INNOVATIVE SCIENCE AND TECHNOLOGY DIRECTORATE
OF STRATEGIC DEFENSE INITIATIVE ORGANIZATION

Contracting Officer's Technical Representative
Dr. Paul Kepple Code 4720
Naval Research Laboratory
4555 Overlook Avenue, SW
Washington, DC 20375-5000

SECURITY CLASSIFICATION OF THIS PAGE *(When Data Entered)*

REPORT DOCUMENTATION PAGE

READ INSTRUCTIONS BEFORE COMPLETING FORM

1. REPORT NUMBER: GRL/8804	2. GOVT ACCESSION NO.
3. RECIPIENT'S CATALOG NUMBER	
4. TITLE *(and Subtitle)*: PROOF OF THE FEASIBIILITY OF COHERENT AND INCOHERENT SCHEMES FOR PUMPING A GAMMA-RAY LASER	5. TYPE OF REPORT & PERIOD COVERED: Quarterly Technical Progress 01/01/89 - 03/31/89
	6. PERFORMING ORG. REPORT NUMBER
7. AUTHOR(s): C. B. Collins	8. CONTRACT OR GRANT NUMBER(s): N00014-86-C-2488
9. PERFORMING ORGANIZATION NAME AND ADDRESS: University of Texas at Dallas, Center for Quantum Electronics, P.O. Box 830688, Richardson, TX 75083-0688	10. PROGRAM ELEMENT, PROJECT, TASK AREA & WORK UNIT NUMBERS
11. CONTROLLING OFFICE NAME AND ADDRESS: INNOVATIVE SCIENCE AND TECHNOLOGY DIRECTORATE OF STRATEGIC DEFENSE INITIATIVE ORGANIZATION	12. REPORT DATE: April 1989
	13. NUMBER OF PAGES: 71
14. MONITORING AGENCY NAME & ADDRESS *(if different from Controlling Office)*: Dr. Paul Kepple, Naval Research Laboratory, Code 4720, 4555 Overlook Avenue, SW, Washington, DC 20375-5000	15. SECURITY CLASS. *(of this report)*: Unclassified
	15a. DECLASSIFICATION/DOWNGRADING SCHEDULE

16. DISTRIBUTION STATEMENT *(of this Report)*

This document has been approved for public release and sale; its distribution is unlimited.

17. DISTRIBUTION STATEMENT *(of the abstract entered in Block 20, if different from Report)*

18. SUPPLEMENTARY NOTES

19. KEY WORDS *(Continue on reverse side if necessary and identify by block number)*

20. ABSTRACT *(Continue on reverse side if necessary and identify by block number)*

Recent approaches to the problem of the gamma-ray laser have focused upon upconversion techniques in which metastable nuclei are pumped with long wavelength radiation. At the nuclear level the storage of energy can approach tera-Joules (10^{12}J) per liter for thousands of years. However, any plan to use such a resource for a gamma-ray laser poses problems of a broad interdisciplinary
(continued on next page)

DD FORM 1473 EDITION OF 1 NOV 65 IS OBSOLETE

SECURITY CLASSIFICATION OF THIS PAGE *(When Data Entered)*

20. Abstract (continued)

nature requiring the fusion of concepts taken from relatively unrelated fields of physics. Our research group has described several means through which this energy might be coupled to the radiation fields with cross sections for stimulated emission that could reach 10^{-17} cm^2. Such a stimulated release could lead to output powers as great as 3×10^{21} Watts/liter. Since 1978 we have pursued an approach for the upconversion of longer wavelength radiation incident upon isomeric nuclear populations that can avoid many of the difficulties encountered with traditional concepts of single photon pumping. Recent experiments have confirmed the general theory and have indicated that a gamma-ray laser is feasible if the right combination of energy levels and branching ratios exists in some real material. Of the 1,886 distinguishable nuclear materials, the present state-of-the-art has been adequate to identify 29 first-class candidates, but further evaluation cannot proceed without remeasurements of nuclear properties with higher precision. A laser-grade database of nuclear properties does not yet exist, but the techniques for constructing one have been developed under this contract and are now being utilized. Resolution of the question of the feasibility of a gamma-ray laser now rests upon the determination of: 1) the identity of the best candidate, 2) the threshold level of laser output, and 3) the upconversion driver for that material.

This quarter's report focuses upon continued success enjoyed along the approach to the gamma-ray laser that depends upon incoherent pumping. This nuclear analog of the ruby laser embodies the simplest concept for a gamma-ray laser and it is not surprising that the greatest rate of achievement toward a sub-Angstrom laser has continued in this direction. Emphasis has remained upon the giant pumping resonances that enabled us to dump populations of the only available sample of the 29 candidates, $^{180}Ta^{m}$, through a cross section that was 10,000 times more favorable than even the most optimistic estimates. The lessons taught by that major milestone have been extended throughout the region of mass-180 nuclides. Reported this quarter is success in pumping the only two of the candidates that are accidentally available, together with 17 other comparison isomers with the bremsstrahlung x-rays from a 4 MeV linac. Previous excitations of the giant resonances pumping these materials had been made with a continuum of photon energies reaching to 6 MeV and concern had lingered that the full 6 MeV of energy might have been actually needed. At such values the density of nuclear states is high and the onset of evaporation of particles from nuclei is near. Either would make the resonances useless to laser development. The significance of this quarter's work is that neither detrimental effect can occur at energies as low as the value of 4 MeV at which performance has now been achieved.

TABLE OF CONTENTS

PREFACE.....i

MAJOR MILESTONE REPORT.....iii

PHOTOEXCITATION OF NUCLEAR ISOMERS BY (γ,γ') REACTIONS THROUGH RELATIVELY UNHINDERED TRANSITIONS ACCESSED WITH BREMSSTRAHLUNG FROM MEDICAL LINEAR ACCELERATORS
by J. J. Carroll, J. A. Anderson, M. J. Byrd, K. N. Taylor, D. G. Richmond, T. W. Sinor, W. L. Hodge, Y. Paiss, C. D. Eberhard and C. B. Collins
University of Texas at Dallas

and E. C. Scarbrough and P. P. Antich
University of Texas Southwestern Medical Center

Introduction.....1
Analytical Method.....4
Experimental Methods and Results.....5
Conclusions.....26
References.....29

LIMITS ON NEUTRON ACTIVATION INTERFERENCES IN PHOTOACTIVATION CROSS-SECTION MEASUREMENTS IN THE 1.5-6 MeV RANGE
by J. A. Anderson, C. D. Eberhard, J. J. Carroll, M. J. Byrd, and C. B. Collins
University of Texas at Dallas

and E. C. Scarbrough and P. P. Antich
University of Texas Southwestern Medical Center

Introduction.....33
Photoneutron Sources.....39
Fast Neutron Flux Measurements.....46
Thermal Neutron Measurements.....51
Conclusions.....58
References.....59

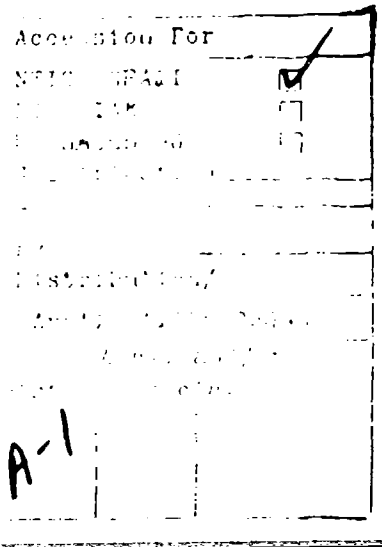

PREFACE

Emphasis this quarter continues to focus upon the successes enjoyed along the approach to the gamma-ray laser that depends upon incoherent pumping. There is embodied the very simplest concept for a gamma-ray laser and it is no surprise that the greatest rate of achievement has been sustained in that direction.

Last year we had first reported the giant resonance for the dumping of the $^{180}Ta^{m}$ isomer by pumping samples with flash x-rays of relatively modest intensities from a 6 MeV linac in a scheme which is the nuclear analog of the ruby laser. This particular material, the worst of the 29 actual candidates, showed what was at that time the largest integrated cross section ever reported for interband transfer in any nuclear material, 4×10^{-22} cm^2 eV. This was an enormous value for bandwidth funneling to a fluorescent level, corresponding to about 0.5 eV of useful width for the absorption of the pump x-rays. Subsequent studies showed that these giant pumping resonances occurred with a gratifying frequency throughout the table of nuclides. However, concern had lingered that these seemingly favorable structures might lie at high energies of excitation near the threshold for neutron evaporation, and so be associated in some way with the high density of nuclear states expected there. This has not proven to be the case.

Highlighted this quarter are the details of a major milestone achievement. *Nineteen isomers were successfully pumped with the bremsstrahlung from a 4 MeV linac.* The density of nuclear states near 4 MeV should be exponentially reduced from values expected near 6 MeV, and yet most isomers were excited with comparable efficiencies by linacs operated at the two energies. The two poorest of the 29 candidates for a gamma-ray laser, $^{180}Ta^{m}$ and $^{123}Te^{m}$, showed the least variation in excitation when the endpoint of the bremsstrahlung was lowered from 6 to 4 MeV. Still, no other candidates are available, but results for these two would encourage expectations that the great width associated with pumping candidate isomers is concentrated at relatively few discrete transition energies.

As usual with these experiments, no significant contributions were made by spurious neutrons evaporated from environmental materials. Although this point has been made in the past, contemporary discussions of the giant resonances for pumping (γ,γ') reactions often still become

concerned with potential neutron contaminations. Reprinted in this report for convenience is an early report which documented the exhaustive attention that had been paid to the elimination of this problem in the irradiation environment produced with the 6 MeV linac. At 4 MeV the possibilities for neutrons to contribute activation are even more reduced; shrinking from th. f_w tenths of a percent that characterized the 6 MeV work to completely negligible values.

As has been the case since 1982, there are still no known factors which inhibit the realization of a gamma-ray laser. Neither the level of pump fluence required for laser threshold nor the waste heat to reject presents any particular problem in idealized materials. *A gamma-ray laser is feasible if the right combination of energy levels occurs in some real material.* When actually tested, the two poorest of the 29 candidate nuclei did surprisingly well, performing 1,000 to 10,000 times better than expected. The overriding question in resolving the feasibility of the nuclear analog to the ruby laser is whether or not one of the better of the 29 has its isomeric level in a position sufficiently near the ideal.

Continuing the preparation of this report as an "in-house" journal, this series presents material to reflect the individual contributions of the teams of research faculty and graduate students involved in these phases of the research. In this regard, I wish to thank all our staff for their splendid efforts in supporting the preparation of these manuscripts to a rather demanding timetable.

- C. B. Collins
- Director
- Center for Quantum Electronics

MAJOR MILESTONE REPORT

Strengthening the Feasibility of a Gamma-Ray Laser

March 21, 1989

C. B. Collins, Center for Quantum Electronics, University of Texas at Dallas

Achievement

Discovered in the first two of the 29 candidate isomers to be tested for a gamma-ray laser were giant pumping resonances which enabled performances to approach the ideal when used with hard x-ray pump sources. Now, these same resonances have been excited with much softer x-rays emitted by a 4 MeV linac.

Technical Background

The nuclear analog of the ruby laser embodies the simplest concepts for a gamma-ray laser. Not surprisingly, the greatest rate of achievement in the quest for a subAngstrom laser continues in that direction. For ruby the identification and exploitation of a bandwidth funnel were the critical keys in the development of the first laser. There was a broad absorption band linked through efficient cascading to the narrow laser level.

Last year we reported a major milestone which showed that comparable structure existed at the nuclear scale in the first of the 29 candidate isomers available for testing, $^{180}Ta^{m}$. Populations of the isomer were successfully pumped down with flashes of x-rays absorbed through an astonishingly large cross section of 40,000 on the usual scale ($\times 10^{-29}$ cm^2 keV) where 10 describes a fully allowed process. This corresponded to a partial width for useful absorption of 0.5 eV, even better than what had been assumed for idealized nuclei. Then we discovered that these giant funnels for pumping isomers occurred rather frequently. We found them in the second of the 29 candidates, $^{123}Te^{m}$, as well as in other demonstration nuclei such as ^{197}Au and ^{195}Pt. However, until now, no experiment could pinpoint the location of such giant resonances in the scheme of energy levels for any of the candidate isomers nor determine whether they lay at small enough energies to be practical.

Reported here is success in pumping the two candidate isomers, $^{180}Ta^{m}$ and $^{123}Te^{m}$ with a 4 MeV linac through the same giant gateways that had been previously accessed with a 6 MeV device.

Report

The inability to vary the spectrum of the x-rays pumping the isomers generally prevent us from locating the precise energies necessary to reach the giant resonances. The spectrum of intensities previously used was the bremsstrahlung from a 6 MeV linac shown in Fig. 1. In this major milestone experiment we obtained another spectral distribution as seen in Fig. 1 from a 4 MeV linac.

Samples with relatively short-lived signatures were run in pneumatic shuttles through the linac x-rays and into the well of a NaI(Tl) crystal where the pumped nuclei were detected. Materials with longer-lived signatures were simply carried to the counting chamber after the pumping terminated. Some non-candidate control nuclei, such as ^{77}Se and ^{89}Y, could only be activated through giant resonances by the 6 MeV linac. However, to within uncertainties in the spectral intensities from the two sources the same levels of activation per unit dose were found in changing from one linac to the other for both the candidates, ^{180}Ta and ^{123}Te. This means that the giant resonances for pumping those two candidates lie at the lower energies common to both pump sources.

Significance

There is a threefold significance to this milestone result.

1) **The giant resonances for pumping the candidate isomers $^{180}Ta^{m}$ and $^{123}Te^{m}$ can be reached at gateway energies well below 4 MeV. These candidates have the largest integrated cross sections for pumping with x-rays ever found below 4 MeV in any nuclei.**

2) **Concern had lingered that the giant pumping resonances previously found with the 6 MeV linac might need the full 6 MeV of energy for excitation. At such values the density of states is high and the onset of evaporation of particles from nuclei is near. Either would make the resonances useless to laser development but neither detrimental effect can occur at energies as low as 4 MeV.**

3) **The two poorest of the 29 candidates are the only ones available for testing and they continue to outperform even the most optimistic expectations. The likelihood for the full feasibility of one of the better candidates continues to be raised by the successes enjoyed with the least attractive of the 29 candidates.**

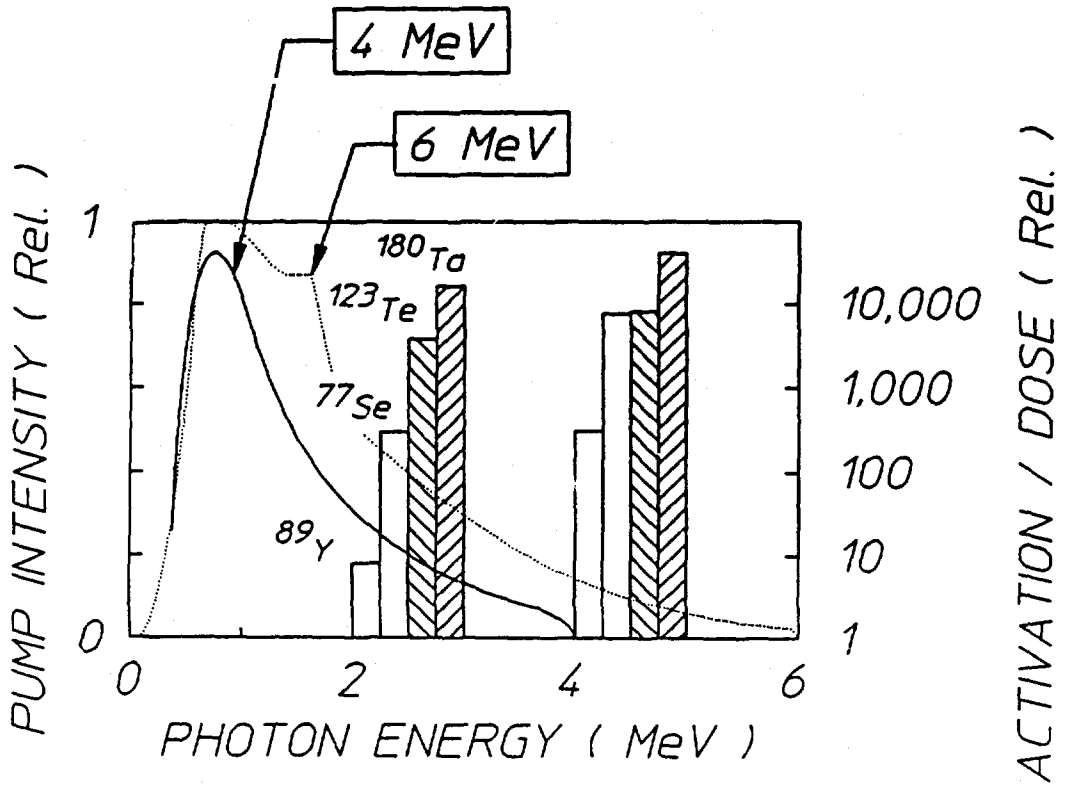

Figure 1: Solid and dotted curves plot the relative spectral intensities in photons/cm^2/keV/sec as functions of photon energies that are expected from the two linac sources identified by the endpoint energies used in these experiments. Bars plot the isomeric activation, or deactivation in the case of $^{180}Ta^{m}$, on the rightmost scale as determined from the nuclear fluorescence observed after pumping with x-rays from the linacs. The leftmost set of bars give results from the 4 MeV linac and the rightmost were obtained with the 6 MeV source. Precise values of the gateway energies remain unknown and the placement of the bars is only to indicate that they lie below 4 or 6 MeV, respectively. Hatched bars identify actual candidate isomers and open bars pertain to non-candidate comparison nuclides.

PHOTOACTIVATION OF NUCLEAR ISOMERS BY (γ,γ') REACTIONS THROUGH RELATIVELY UNHINDERED TRANSITIONS ACCESSED WITH BREMSSTRAHLUNG FROM MEDICAL LINEAR ACCELERATORS

by J. J. Carroll, J. A. Anderson, M. J. Byrd, K. N. Taylor, D. G. Richmond, T. W. Sinor, W. L. Hodge, Y. Paiss, C. D. Eberhard and C. B. Collins

Center for Quantum Electronics, University of Texas at Dallas

and E. C. Scarbrough and P. P. Antich

University of Texas Southwestern Medical Center

Introduction

The photoexcitation of isomeric nuclei through (γ,γ') reactions has been investigated for more than fifty years.[1,2] Surprisingly there is very little convergence among the few tens of experimental results that have been published in this time.[3] The extreme variance between measurements is surprising when compared with the precision routinely achieved in the examination of all types of particle reactions. Moreover, the analogous optical double resonance technique is among the most powerful methods of investigation at the molecular level. Nevertheless, (γ,γ') studies have provided widely differing results as exemplified by investigations of the reactions $^{111}Cd(\gamma,\gamma')^{111}Cd^{m}$ and $^{115}In(\gamma,\gamma')^{115}In^{m}$.

The stable nuclide ^{111}Cd would seem to be nearly ideal for nuclear fluorescence studies due to the readily observable lines at 150.6 and 245.5 keV radiated from its 396 keV isomer and the moderate isomeric half-life of 48.6 min.[4,5] Only slightly less convenient is the isomer $^{115}In^{m}$, having a half-life of 269 min and a fluorescence line at 336 keV, the isomeric energy. A variety of irradiations using either radioactive ^{60}Co or ^{137}Cs sources or bremsstrahlung from accelerators have been performed to activate samples containing these nuclei at energies up to about 1.5 MeV. Each of these sources was intense enough to excite sufficient numbers of nuclei to insure reasonable counting statistics and good signal-to-noise ratios. However, in several carefully conducted experiments[6,7,8] values of the integrated cross-section for the photoexcitation of $^{111}Cd^{m}$ were found to range from 5.8 ± 0.8 to 35 ± 4 in

the usual units of 10^{-29} cm^2-keV. Likewise, values for $^{115}In^m$ were found[9,10] to range from 5.38 ± 0.64 to 23 ± 4 in the same units.

It has been generally thought that (γ,γ') reactions occur through resonant processes. However, in attempting to explain the seemingly excess activations observed in some experiments, several investigators[7,9] have postulated that the photoexcitation proceeded instead through a non-resonant channel. Theory has never been able to supply a mechanism of sufficient magnitude to account for this behavior at energies below 1.5 MeV but the idea remained a controversial[3] alternative to resonant excitation for some time.

Recently the technology has become available[11,12] to measure directly the spectrum of a variable energy source of pulsed bremsstrahlung in the 0.5 to 1.5 MeV range. With such a device, the DNA/PITHON nuclear simulator at Physics International, it was found[13,14] that both $^{115}In^m$ and $^{111}Cd^m$ were excited by predominantly resonant absorption through intermediate states, called gateway states, near 1 MeV which were broadened by their relatively short lifetimes. The sharp onset of the (γ,γ') reactions with increasing energy relegated to less than 3% any contributions from non-resonant processes and indicated that the gateway states were reasonably well connected by radiative transitions to both the ground states and the isomers. It appears that the principle cause for the large discrepancy between previous measurements was the difficulty in adequately characterizing the spectra of the irradiating sources. This is particularly true for radioactive line sources since all spectral contributions off the resonance line are due to Compton continua generated by environmentally-sensitive radiation transport processes.

The identification of relatively narrow gateway states below 1.5 MeV for the photoexcitation of isomers and the measurement of their cross-sections has reopened the question of the existence of similar gateways in the region from 1.5 to 6 MeV. In this energy range very early data[15,16] indicated that yields from (γ,γ') reactions increased as mediating states were accessed at higher energies. Evidence was accumulated in the form of increases in the slopes of curves showing isomeric yields as functions of the endpoint energies of the bremsstrahlung used to pump the reactions, but the changes were not dramatic. The largest value found[16] was $580 \cdot 10^{-29}$ cm^2-keV for the photoexcitation of $^{87}Sr^m$ through a gateway at 2.66 MeV.

A renaissance in the study of (γ,γ') reactions has been launched by the availability of medical linear accelerators which can serve as intense and stable bremsstrahlung sources. The total doses which these devices can deposit in reasonable working periods have made possible the examination of reactions involving even rare nuclides for which target masses are limited to milligrams. In this way, the first (γ,γ') reaction leading to the deexcitation of an isomeric sample, $^{180}Ta^{m}(\gamma,\gamma')^{180}Ta$, was studied[17] with unexpected results.

The isomer $^{180}Ta^{m}$ is nature's rarest naturally occurring isotope.[18] Requiring an unlikely change of $\Delta J = 8$, the isomer was dumped to the ground state by bremsstrahlung having an endpoint of about 6 MeV. The partial width for this reaction was found[17] to be at least 0.5 eV, an enormous value exceeding any previous reports for (γ,γ') reactions by two to three orders of magnitude. The amount of deexcitation of the isomer observed was astonishing, corresponding to a total integrated cross-section in excess of $4 \cdot 10^{-25}$ cm^2-keV. Even more recently, this strength of the dumping reaction $^{180}Ta^{m}(\gamma,\gamma')^{180}Ta$ was qualitatively confirmed[19] with bremsstrahlung from the injector to the Darmstadt superconducting electron machine operated at 4.6 MeV. In this work the extension of these results to endpoint energies as low as 4.0 MeV will be described.

In general the endpoint energies of medical linacs cannot be continuously tuned and this presents a severe impediment to the duplication of the kind of detailed successes achieved[10-14] below 1.5 MeV. Nevertheless, experimental results obtained from samples irradiated with this type of device form a foundation for further investigations which might provide better resolution. Reported here are the results of two experimental series in which a variety of isomeric nuclei were excited by irradiating targets with 4 and 6 MeV fixed endpoint linacs.

Analytical Method

The photoexcitation rate for the production of an isomer through a (γ,γ') reaction is given by

$$\frac{dN_{excited}}{dt} = N_T \int_{-\infty}^{\infty} \sigma(E)\ \Phi(E)\ dE, \qquad (1)$$

where $\sigma(E)$ is the cross-section in cm^2, $\Phi(E)$ is the spectral intensity of the pump source in photons/cm^2-keV-sec and N_T is the number of target nuclei. The spectral intensity can be expressed as the product of the total photon flux Φ_o and a relative spectral intensity function F(E). The combination $d/dt(N_{excited}/N_T)$ is commonly referred to as the activation rate. Assuming that the (γ,γ') reactions proceed through resonant mediating states which are narrow relative to any structure of the irradiating source spectrum, as is the case below 1.5 MeV, Eq. 1 becomes

$$\frac{dN_{excited}}{dt} = N_T \sum_i (\sigma\Gamma)_i\ \Phi(E_i). \qquad (2)$$

Here $\Phi(E_i)$ is the photon intensity at the gateway energy E_i and Γ_i is the natural width in keV of the i^{th} mediating state. From the uncertainty principle, $\Gamma_i \geq \hbar/\tau_i$, where τ_i is the lifetime of the state. The quantity $(\sigma\Gamma)_i$ is the integrated cross-section in cm^2-keV and is defined by

$$(\sigma\Gamma)_i = \int_{i^{th}\ resonance} \sigma(E)\ dE. \qquad (3)$$

The integrated cross-section is usually expressed as $\pi b_a b_o \sigma_o \Gamma/2$ where b_a and b_o are the branching ratios for decay from the gateway level to the ground and isomeric states. The product $b_a b_o \Gamma$ is called the partial width for the transition. The quantity σ_o is the amplitude of the Breit-Wigner cross-section for the absorption transition,

$$\sigma_o = \frac{\lambda^2}{2\pi} \frac{I_e + 1}{I_g + 1} \frac{1}{\alpha_p + 1}, \qquad (4)$$

where λ is the wavelength in cm of the γ-ray at the resonant energy, I_e and I_g are the nuclear spins of the excited and ground states, and α_p is the internal conversion coefficient of the absorption transition.

An exact evaluation of the integrated cross-sections in Eq. 2 requires the energy region in question to be scanned by a variable endpoint photon source with a well known spectrum. This was not possible in the current experiments because of the availability of only fixed endpoint medical linacs as pump sources, and thus the results are most accurately quoted in the form of activations normalized to the total photon flux of the irradiating device. However, it was instructive to assume that only one gateway was accessed and to compute its effective integrated cross-section. The integrated cross-section for such a hypothetical state located at energy E is then given by

$$(\sigma\Gamma) = \frac{1}{N_T\ \Phi(E)} \frac{dN_{excited}}{dt}. \qquad (5)$$

The cross-sections of these assumed single gateways was found by experimentally measuring the number of isomers excited during exposure to a source for which $\Phi(E)$ is well known.

Experimental Methods and Results

The irradiation of sample materials was accomplished with the aid of 4 and 6 MeV medical linacs at the Department of Radiology of the University of Texas Southwestern Medical Center at Dallas. Bremsstrahlung having a nominal endpoint of 6 MeV was obtained with a Varian Clinac 1800 linac operating in the 6 MeV mode. This device produced a dose rate of 4 Gy(H_2O)/min at a distance of 101.5 cm from the photon source. The 4 MeV irradiations were performed with a Varian 4/100 linac which provided a dose rate of 2 Gy(H_2O)/min at a distance of 101.2 cm from the photon source. The spectra of these machines have been well characterized[20,21] by use of the established EGS4 code[22] with a resolution of 0.25 MeV. The relative spectral intensity functions F(E) of each linac are shown in Fig 1. For convenience, these numbers are given explicitly in Table I. The absolute spectral intensity was found from the delivered dose by standard techniques.[23] The total flux of the 6 MeV Clinac 1800 beam was $5.35 \cdot 10^{15}$ photons/r^2-min while that of the 4/100 was found to be $3.23 \cdot 10^{15}$ photons/r^2-min. The inclusion of the variable r, the

distance in cm from the target location to the bremsstrahlung source, allowed these values to be adjusted to various sample positions.

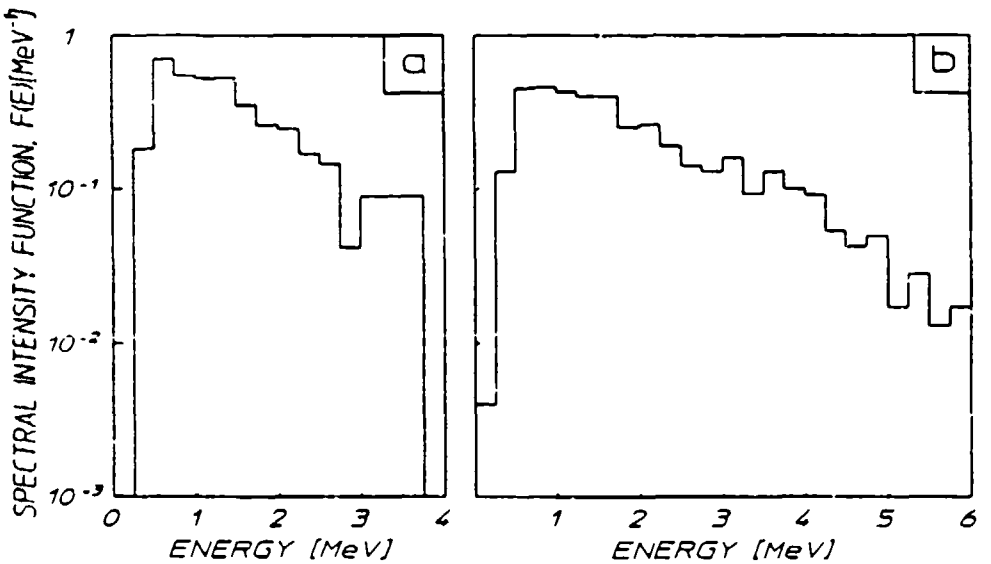

Figure 1: Relative spectral intensity functions F(E) of the bremsstrahlung produced by the medical linear accelerators used to irradiate samples in these experiments. The plots are normalized so that the integral under the curves is unity. The devices employed were:
a) Varian 4/100, with nominal endpoint energy of 4 MeV.
b) Varian Clinac 1800, operated in the nominal 6 MeV endpoint energy mode.

Table I

Relative spectral intensity function F(E) for the two medical linacs used in these experiments.

Energy [MeV]	4 MeV Linac F(E) [MeV^{-1}]	6 MeV Linac F(E) [MeV^{-1}]
0.125	0.001	0.004
0.375	0.180	0.130
0 625	0.711	0.450
0.875	0.549	0.460
1.125	0.524	0.430
1.375	0.529	0.400
1.625	0.350	0.400
1.875	0.258	0.250
2.125	0.246	0.260
2.375	0.168	0.190
2.625	0.145	0.140
2.875	0.041	0.130
3.125	0.089	0.160
3.375	0.089	0.092
3.625	0.089	0.130
3.875	0.001	0.100
4.125		0.090
4.375		0.053
4.625		0.042
4.875		0.049
5.125		0.017
5.375		0.028
5.625		0.013
5.875		0.017

The isotopes studied in these experiments are listed in Table II along with some relevant physical parameters. For each nuclide, the excitation rate was calculated from the number of isomeric decays observed in the samples following irradiation. This was reflected by the total counts in the full energy peaks of the isomeric fluorescence lines. These observations were corrected for detector efficiency, fluorescence intensity and the finite periods of exposure and counting. The latter factors used literature values for the half-lives of the isomers.[24] The samples were essentially transparent at the pump energies, but at the fluorescence energies some self-absorption was possible. A further correction which accommodated non-unity transparencies was calculated by Monte-Carlo methods for each sample. These calculations were tested by comparing the cross-sections obtained from samples containing identical materials, but in different geometries. The experimental methods employed to measure the activity present in each sample fall into three categories due to the physical properties of the nuclei. In the interest of brevity, these measurements will be illustrated in detail by an example of each technique.

The first nine nuclides listed in Table II have half-lives of less than about 153 sec. These samples therefore consisted of either powders or metallic foils enclosed in cylindrical polyethylene vials, termed rabbits, which could be pneumatically transported to a NaI(Tl) detector after individual exposures. The low energy resolution of the NaI(Tl) detector necessitated some care in the identification of the prominent features in the pulse height spectra obtained. Confirmation that these features were indeed the fluorescence signatures of the isomers present was made by determining the half-lives of these lines and comparing them with literature values. Data was simultaneously acquired through two Ortec 918A ADCAM multichannel buffers controlled by a personal computer. Thus, while one ADCAM served to produce a pulse height spectrum, the other collected a record of the total counts received in a preset dwell interval as a function of time.

Table II

Summary of isomeric nuclei studied. Nuclei marked * were present in isotopically enriched samples. In the sample column, R refers to samples contained in rabbits, P to flat planchettes, F to metallic foils, and B to scintillation bottles. The ^{180}Ta sample consisted of a dusting of oxide on a thin aluminum plate, referred to by D. In the case of the ^{176}Lu sample, β^- particles were observed instead of fluorescence photons; the NA in the transparency column indicates that this factor was not applicable for ^{176}Lu.

Nuclide	Abundance [%]	Sample Form	$T_{1/2}$	Principle Fluorescence [keV]	Transparency
^{167}Er	91.54 *	Er_2O_3 (R)	2.28 sec	207.79 (41.70%)	57.90
^{79}Br	50.69	LiBr (R)	4.86 sec	207.20 (75.80%)	84.90
^{191}Ir	37.30	Ir (R)	4.94 sec	129.43 (25.70%)	10.50
^{197}Au	100.00	Au (R)	7.80 sec	279.11 (73.00%)	92.70
^{89}Y	100.00	YF_3 (R)	16.06 sec	909.15 (99.14%)	94.70
^{77}Se	94.38	Se (R)	17.45 sec	161.92 (52.40%)	72.28
^{179}Hf	13.63	HfO_2 (R)	18.68 sec	214.31 (94.20%)	52.40
^{199}Hg	16.90	Hg_2Cl_2 (R)	43.20 sec	158.40 (53.00%)	43.96
^{137}Ba	11.74	BaF_2 (R)	153.12 sec	661.66 (90.10%)	95.50
^{111}Cd	12.80	Cd (F)	48.6 min	245.49 (94.00%)	76.35
^{113}In	4.30	In (F)	1.66 hr	391.69 (64.20%)	98.30
^{87}Sr	7.00	SrF_2 (P)	2.81 hr	388.40 (82.30%)	95.78
^{176}Lu	2.59	$LuCl_2$ (B)	3.63 hr	beta	NA
^{115}In	95.70	In (F)	4.49 hr	336.26 (45.80%)	98.00
^{180}Ta	4.00 *	TaO_2 (D)	8.15 hr	55.79 (36.00%)	100.00
^{135}Ba	6.60	BaF_2 (P)	1.20 d	268.27 (15.60%)	94.33
^{195}Pt	33.80	Pt (Coin)	4.02 d	98.88 (11.40%)	4.76
^{117}Sn	7.70	Sn (F)	13.6 d	158.56 (86.40%)	92.89
^{123}Te	0.908	Te (P)	119.7 d	158.99 (84.00%)	62.68

A typical example of the data obtained in this way is given in Figs. 2 and 3, showing the pulse height and time spectra measured for the isomer $^{167}Er^{m}$. The total number of counts in the full energy peak at 207.8 keV was determined with a commercially available data reduction package. The information was then used to evaluate the integrated cross-section as a function of assumed gateway energy for both 4 and 6 MeV irradiations as shown in Fig. 4. The values shown in this graph have been corrected for the very small amounts of slow neutron contamination as discussed below.

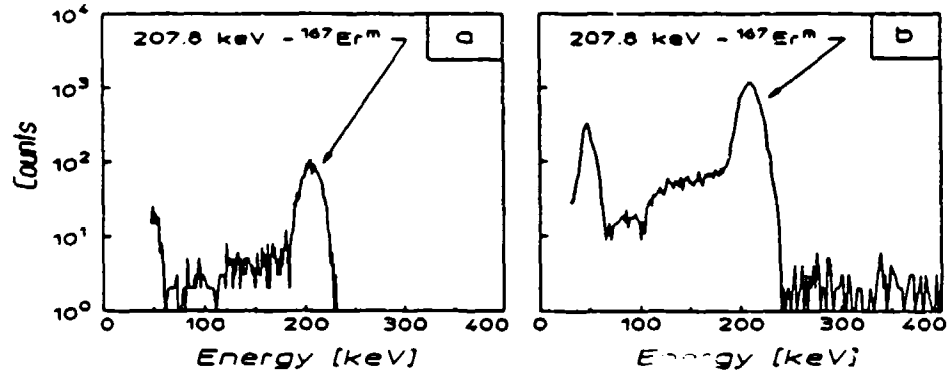

Figure 2: Pulse height spectra showing the 207.8 keV fluorescence line from the decay of $^{167}Er^{m}$. These spectra were obtained with a 7.6 cm × 7.6 cm diameter NaI(Tl) detector having a 5.1 cm × 2.5 cm diameter well. The samples were irradiated for 25 sec and the counting periods were 5 sec in duration. The endpoint energies of the bremsstrahlung used to activate the samples and the delay times from the end of irradiation to the start of counting were:
a) 4 MeV exposure, delay of 1.583 sec.
b) 6 MeV exposure, delay of 2.060 sec.

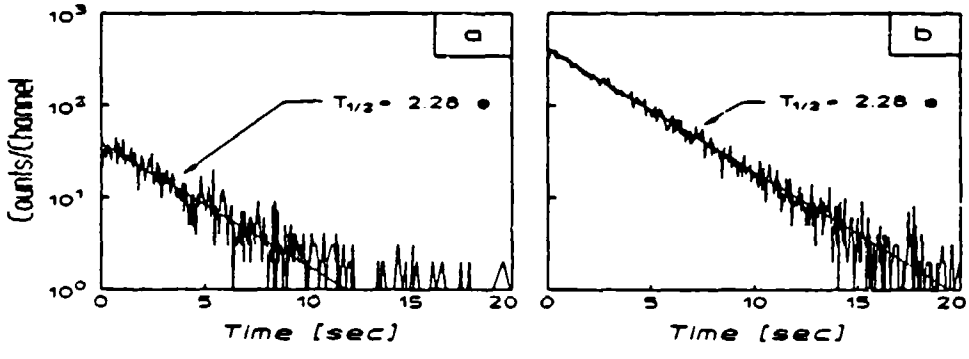

Figure 3: Time decay spectra of the total counting rate as a function of the time elapsed from the start of counting for $^{167}Er^{m}$. The solid lines indicate the decay expected from the literature value of the half-life, 2.28 sec. The spectra were obtained by recording the number of counts observed in successive dwell intervals of 0.05 sec with a multichannel scalar. The counting device was a 7.6 cm × 7.6 cm diameter NaI(Tl) detector having a 5.1 cm × 2.5 cm diameter well. All events above a chosen lower level discriminator were measured for samples after the following exposures:
a) 4 MeV exposure, delay of 1.583 sec.
b) 6 MeV exposure, delay of 2.060 sec.

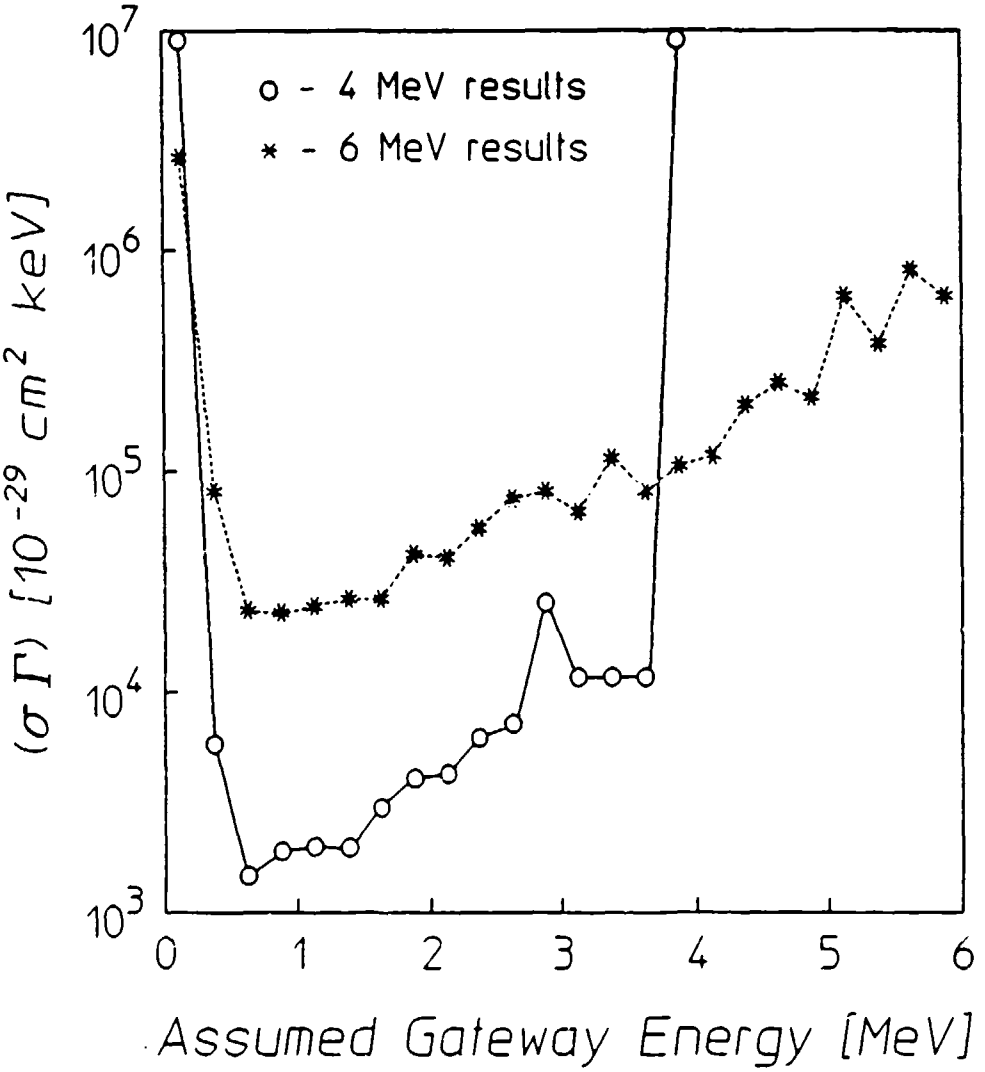

Figure 4: Integrated cross-sections for the reaction $^{167}Er(\gamma,\gamma')^{167}Er^m$ through single, unknown gateway states as functions of the energies at which these states could be assumed to lie. The circles indicate the results of measurements using the 4 MeV linac while the asterisks show those from the 6 MeV experiments.

A second experimental method was used to investigate the remaining nuclides in Table II, with the exception of ^{176}Lu. All of these have half-lives longer than 48.6 min, which allowed the samples to be irradiated in complex packages placed perpendicular to the photon beam. The packages were exposed for periods of up to four hours, removed by hand from the linac chambers at the end of the irradiations, and transported to the Center for Quantum Electronics at the University of Texas at Dallas for counting.

The measurements of the observed activities were made with a 10% relative efficiency, n-type germanium detector. Because of the higher energy resolution of this type of detector it was not necessary to monitor the time decay in detail for these samples although in some cases energy spectra were acquired after several different elapsed times. This second type of measurement is typified by the examination of the isomer $^{123}Te^{m}$, which has a half-life of 119.7 days. Pulse height spectra following 4 and 6 MeV exposures are shown in Fig. 5. The fluorescence line at 159 keV was well defined in spectra excited with both 4 and 6 MeV linacs, and good counting statistics were observed. This was rewarding since there was some concern that the activation of such a long-lived isomer might be hidden by the natural background of the counting chamber. Nevertheless, since this is the longest-lived isomer ever reported to be excited by a (γ,γ') reaction, the time decay was experimentally determined from a sequence of energy spectra taken following a 6 MeV exposure. The count rate was observed in the fluorescence peak as a function of time as shown in Fig. 6 and the literature value of the half-life of $^{123}Te^{m}$ was in good agreement with this data. The resulting integrated cross-sections are displayed in Fig. 7, again corrected for very small amounts of neutron contamination.

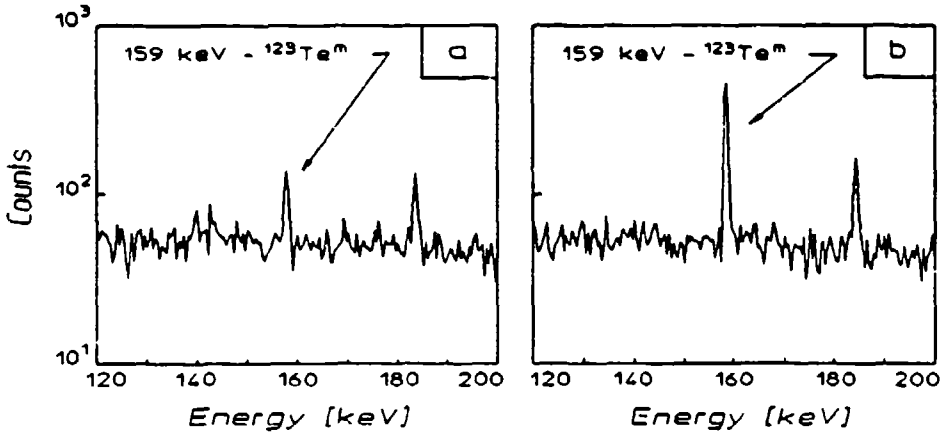

Figure 5: Pulse height spectra showing the 159 keV fluorescence line from the decay of $^{123}Te^{m}$. The spectra were obtained with an n-type high purity germanium detector. The samples were irradiated for 2 hours and the counting periods were 10 hours in duration. The endpoint energies of the bremsstrahlung used to activate the samples and the delay times from the end of irradiation ot the start of counting were:
a) 4 MeV exposure, delay of 43.91 hours.
b) 6 MeV exposure, delay of 22.98 hours.

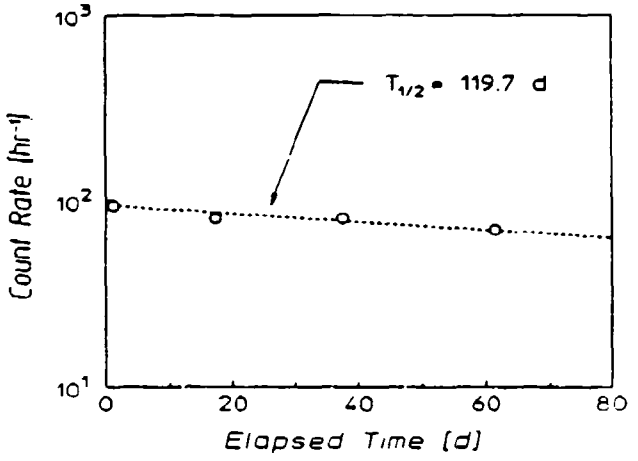

Figure 6: Plot of the time decay of the 159 keV fluorescence line from the decay of $^{123}Te^{m}$ following exposure to bremsstrahlung from the 6 MeV linac. The points represent the counting rate observed in several pulse height spectra obtained at different elapsed times. The size of the symbols is comparable to one standard deviation and the counting periods were of 10 hour duration. The dashed line indicates the expected decay half-life of 119.7 days, taken from the literature, and is in good agreement with the measurements.

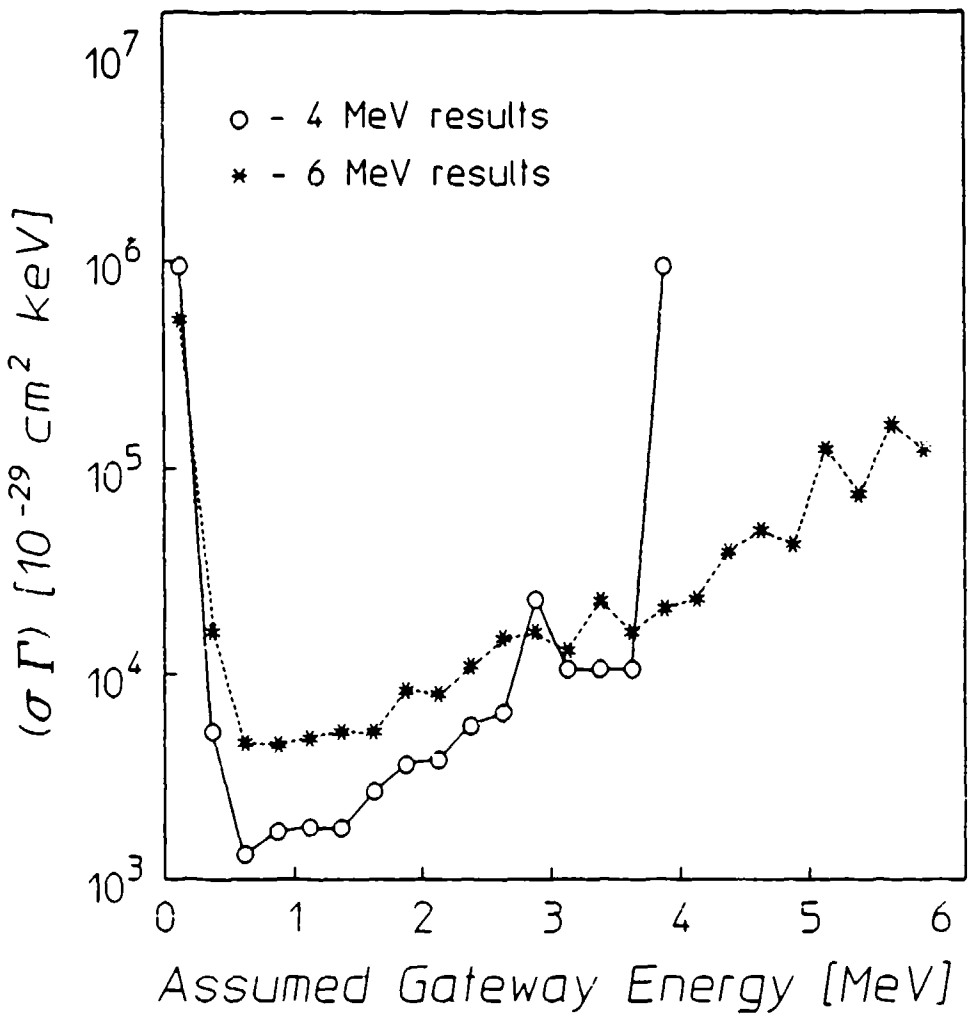

Figure 7: Integrated cross-sections for the reaction $^{123}Te(\gamma,\gamma')^{123}Te^m$ through single, unknown gateway states as functions of the energies at which these states could be assumed to lie. The circles indicate the results of measurements using the 4 MeV linac while the asterisks show those from the 6 MeV experiments.

The remaining nuclide, ^{176}Lu, was examined with a third detection scheme. The ground state of this isotope β^- decays with an endpoint energy of 565 keV and the isomer β^- decays with endpoint energies of 1313 keV (39.6%) and 1225 keV (60.4%). Since the isomer does not return to the ground state by a radiative transition, the number of excited nuclei must be measured by the detection of either the β^- particles or the signature photons from the daughter nucleus. This type of deexcitation process is similar to that of ^{180}Ta, which decays by both electron capture and β^- modes.

In the case of ^{176}Lu, the decay energies allowed the use of a Cerenkov detector. Samples consisting of 5 g of $LuCl_3$, dissolved in distilled water to make about 20 ml of solution, were contained in polyethylene scintillation bottles. The Cerenkov threshold in water is about 250 keV; β^- particles emitted in the decay of the isomeric states were nearly 10 times more efficient in producing Cerenkov events than those emitted from ground state nuclei. These events were measured by a system consisting of two RCA 8850 photomultiplier tubes in EG & G bases. The tubes were used in a coincidence mode by connecting their time synchronized outputs through a 150 MHz Phillips 755 logic unit, thereby recognizing only coincident signals from the Cerenkov photons produced by single β^- particles. These were recorded as a function of elapsed time in multichannel scalar spectra where each channel represented a dwell time of 40 sec. The detector was calibrated with ^{40}K decays from a KCl solution of known activity. The β^- particles resulting from ^{40}K decay have roughly the same endpoint energy as from $^{176}Lu^m$. In these measurements, the individual count rates were monitored to avoid contributions from accidental coincidences triggered by separate β^- events or by thermoluminescence from the bottle. A fit to the experimental data shown in the typical spectrum of Fig. 8 produced a value for the half-life of $^{176}Lu^m$, 3.58 $\pm$ 0.05 hours, which was in good agreement with the literature value of 3.63 hours. The integrated cross-section as a function of gateway energy was calculated from the activation present immediately after irradiation and is shown in Fig. 9.

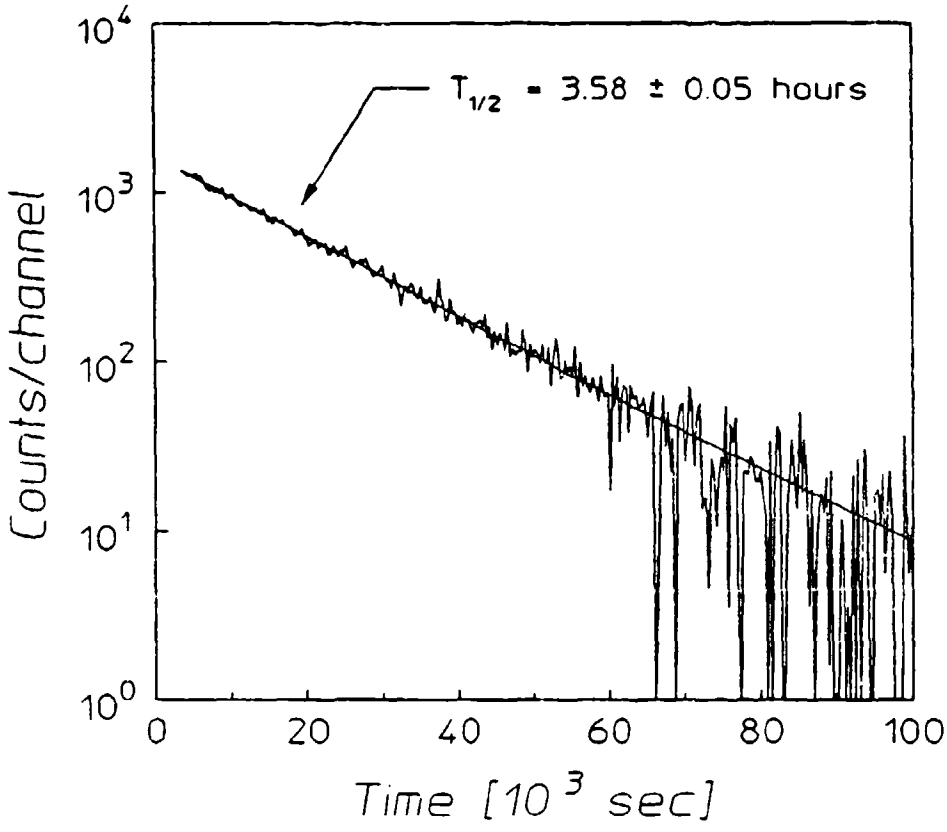

Figure 8: Time decay spectrum of the total counting rate as a function of the time elapsed from the start of counting for $^{176}Lu^m$ following a 6 MeV exposure. This was obtained by recording the number of counts observed in successive dwell intervals of 320 sec with a multichannel scalar. The device used to make these measurements consisted of two RCA 8850 photomultiplier tubes operated in a coincidence mode. Samples were composed of $LuCl_3$ dissolved in distilled water in plastic bottles. The observed decay signatures were β^- particles which were detected from the Cerenkov radiation produced in the water. The sample was irradiated for 40 minutes and the delay time was 53 minutes. A fit to the data is shown by the solid line and gives a half-life of 3.58 ± 0.05 hours, in good agreement with the literature value of 3.63 hours.

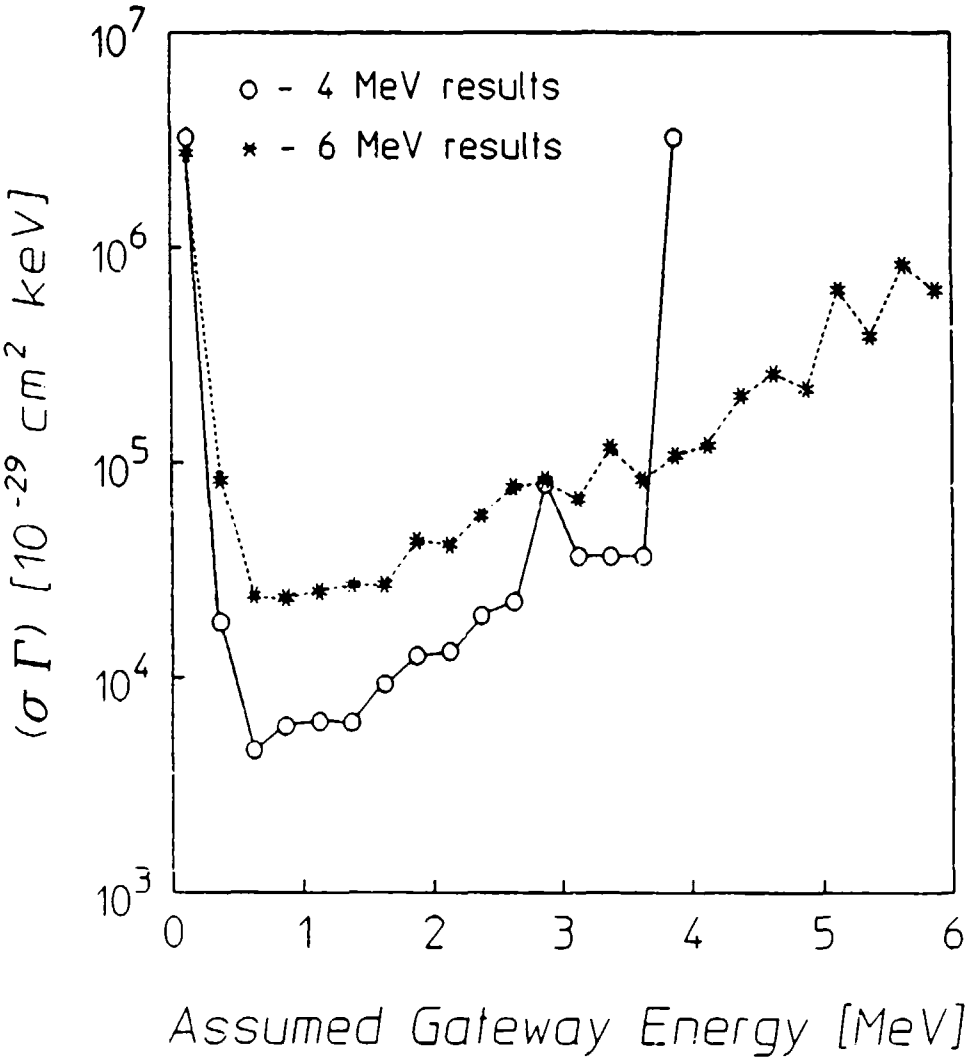

Figure 9: Integrated cross-sections for the reaction $^{176}Lu(\gamma,\gamma')^{176}Lu^m$ through single, unknown gateway states as functions of the energies at which these states could be assumed to lie. The circles indicate the results of measurements using the 4 MeV linac while the asterisks show those from the 6 MeV experiments.

Since the high energy photons used in these experiments were capable of evaporating neutrons from some materials, the possibility of neutron excitation of the isomeric populations had to be carefully considered. The principal objective of this study was to characterize (γ,γ') reactions in the energy range from 1.5 to 6 MeV. Thus any contributions to the yield from processes indirectly mediated by neutrons would have appeared as unwanted contaminations of the photoexcitation cross-sections finally obtained. In principle, two types of neutron reactions could have occurred: inelastic (n,n') reactions which would have required hot neutrons and neutron capture (n,γ) processes driven by any fluxes of thermal or epithermal neutrons which might have been present. Both would have required a primary source of neutrons to have been active during the bremsstrahlung irradiation.

Only eight isotopes have thresholds for (γ,n) reactions below 6 MeV. Four of these are rare and can be reasonably excluded from consideration. The materials used in the irradiation device and facility were documented. In these materials only ^{2}H, ^{9}Be, ^{13}C and ^{17}O can be expected to have served as sources of neutrons in the irradiation environment actually used in these experiments.

As the photon intensity was monitored throughout the course of these experiments, the flux of primary photoneutrons can be calculated with reasonable accuracy from the following potential sources:

1) a 0.025 cm thick Be window located below the bremsstrahlung converter target in the 6 MeV linac.

2) the ^{2}H in the cooling water in the bremsstrahlung converter target.

3) the ^{2}H in the humidity in the chamber and the ^{13}C and ^{17}O in the volume of atmosphere incidentally irradiated.

4) the ^{2}N, ^{13}C and ^{17}O in the concrete used in construction.

Of these, the first dominated by orders-of-magnitude, giving an expected flux of 10^{3} neutrons/cm^{2} sec at the position of the experimental samples.

The potential activation produced by such a flux is difficult to estimate because the cross-sections for (n,n') reactions are poorly known. However, if it is assumed that all of the flux carries at least

threshold energy, the cross-section $\sigma_{n,100\%}$ necessary to produce all of the measured activation from all sources of neutrons can be calculated. These resulting values are summarized in Table III in units of barns and values can be seen to range from tens to thousands. This is to be compared with the few hundreds of millibarns that describe (n,n') reactions in those few cases where measurements have been reported in the literature.

Total neutron cross-sections, which certainly must be greater than the inelastic component, are available for all of the materials studied.[25] They are summarized in Table III, together with any other cross-sections which might bound more closely the value expected for the relevant (n,n') reaction producing the observed isomer.[26-33] Finally, in Table III is tabulated the ratio, Ω, which compares the most restrictive upper limit to $\sigma_{n,100\%}$, the cross-section for inelastic neutron excitation which would be necessary to explain all of the observed yield.

In effect Ω is the maximum fractional contamination through the fast neutron channel of the photoexcitation yield. As can be seen, values are generally smaller than 1% and exceptions occur only in cases for which restrictive estimates of (n,n') cross-sections are unavailable.

The fast neutron flux expected in these experiments, 10^3 neutrons/cm^2-sec was too small to confirm by direct measurement in such a high ambient level of photon irradiation. However, in order to completely exclude the remote possibility of an undocumented emplacement of some strong photoneutron source such as ^{235}U in the irradiation environment, a measurement was attempted using standard procedures.[34,35] The (n,p) reactions of ^{46}Ti, ^{47}Ti and ^{58}Ni are well-documented and provide clear signature photons for convenient periods of decay. These nuclei are not affected by the photon beam in this energy range but they are sensitive to fast neutrons, producing the daughters ^{46}Sc, ^{47}Sc and ^{58}Co, respectively.

Table III

Summary of fast neutron contamination limits. The fast neutron cross-section, $\sigma_{n,100\%}$ is that required to produce 100% of the observed activations. Maximum values for the true total neutron cross-section of the element of interest,[25] σ_{tot}, are shown for the energy range 0.1 to 6 MeV. When available, the non-elastic cross-section for the element has been shown in parentheses following the elastic cross-section. The most restrictive additional cross-section, σ_{lim}, for the particular isotope or element is given with its type and E_{max}, the energy up to which it was determined. Cross-section types are as follows: ie - inelastic in element; i - inelastic in isotope; n - non-elastic in isotope; fi - inelastic in isotope, average for fission spectrum. The factor Ω is the ratio of the most specific observed cross-section to the cross-section required for a 100% contamination effect, and thus represents an upper limit for contamination of the neutron effects.

Nuclide	$\sigma_{n,100\%}$ [b]	σ_{tot} [b]	σ_{lim} [b]		Type	E_{max} [MeV]	Ω [%]
^{167}Er	2700	9	-		-	-	0.33
^{79}Br	140	7.5	-		-	-	5.4
^{191}Ir	2590	10.3	-		-	-	0.40
^{197}Au	95	10	1.3	32	i	5.3	1.4
^{89}Y	20	11.5	0.2	27	i	4.0	1.0
^{77}Se	490	8.3(2.4)	0.73	26	fi	-	0.15
^{179}Hf	1940	20	0.4	31	i	1.6	0.02
^{199}Hg	120	10(2.6)	0.14	33	i	2.1	0.12
^{137}Ba	130	7.3(2)	0.66	30	i	3	0.51
^{111}Cd	210	8	0.23	26	fi	-	0.11
^{113}In	320	6.3	0.047	28	i	1.0	0.01
^{87}Sr	60	10	0.11	26	fi	-	0.18
^{176}Lu	2638	7	-		-	-	0.27
^{115}In	430	6.3	0.38	29	i	5.3	0.09
^{180}Ta	3015	8.5(2.9)	1.8	32	ie	1.8	0.06
^{135}Ba	420	7.3(2)	-		-	-	0.48
^{195}Pt	1350	10	0.68	32	ie	1.8	0.05
^{117}Sn	70	6.8(2)	-		-	-	2.9
^{123}Te	530	6	-		-	-	1.1

In this measurement, the foils were irradiated, removed to the HPGe detector system and counted to obtain pulse height spectra. In these spectra no signature photon peaks from the daughters were evidenced at any levels above the background of the counting chamber. It was therefore possible to obtain only an upper bound on the fast neutron flux at the sample position, that of $7 \cdot 10^4$ neutrons/cm^2 sec.

As can be seen, the limit established by measurement is not particularly restrictive, being 70 times larger than the calculated values of fast neutron flux. Nevertheless, even if the limits of contamination in Table III are raised by this factor of 70, at least half of the samples would still be affected by of errors less than 10%. Only in the case of unknown inelestic cross-sections for a (n,n') reaction closely approaching the total values shown in Table III could an undocumented sample of rare material have produced a level of fast neutron flux sufficient to contaminate the results of the (γ,γ') reactions being studied. Such occurrances would have required the coincidence of very improbable circumstances and merit no further consideration. That so little fast neutron contamination occurred due to the 6 MeV linac precluded any possibility of significant effects of fast neutrons in the 4 MeV experiments.

The thermal and epithermal neutron fluxes due to the 6 MeV linac, Φ_{th} and Φ_{ep}, could be measured in this environment by irradiating two thin indium foils, one of which was shielded from thermal neutrons by a cadmium cover. In accordance with standard techniques,[36] energy spectra obtained from these foils were examined after exposure for signature photons from the isomer $^{116}In^{m}$, which is produced by a branch of the reaction $^{115}In(n,\gamma)^{116}In^{m,g}$. The magnitudes of the fluorescence lines observed in both the bare and the shielded samples allowed the determination of the neutron fluxes Φ_{th} = 12 neutrons/cm^2-sec and Φ_{ep} = 6 neutrons/cm^2-sec from literature values of the thermal and epithermal neutron cross-sections.[37] The neutron fluxes from the 4 MeV linac were bounded in a similar way. A bare indium foil was exposed, but later showed no photopeaks from $^{116}In^{m}$ observable above the background. Upper bounds for the neutron fluxes were found by assuming for the 4 MeV environment the same 2:1 ratio of thermal to epithermal neutrons found at 6 MeV. The activation was taken to be just below the level of noise, which gave $\Phi_{th} \leq 6$ neutrons/cm^2-min and $\Phi_{ep} \leq 3$ neutrons/cm^2-min during operation of the 4 MeV linac. The small amount of activation of each of

the isomers due to these neutrons was subtracted from the total activation observed. In no case did the contribution from thermal and epithermal neutrons in the 4 MeV environment exceed 0.05%. The thermal and epithermal neutron fluxes in the 6 MeV chamber produced contributions below 1.51% for all isomers except for $^{179}Hf^{m}$ (6.41%) and $^{199}Hg^{m}$ (5.40%). Even in these materials, it is apparent that photoexcitation is the dominant mechanism for the observed activation.

Limits on the fractional contamination of the (γ,γ') activation of the isomers studied in these experiments are summarized as Ω in Table III for processes initiated by fast neutrons and as A_n/A_{Tot} in Table IV for processes involving slow neutrons. In all cases, the values exceeding 1% are primarily the consequence of poorly bounded neutron cross-sections for the intermediate steps. In those cases the only available values were those describing total processes which certainly bound the (n,n') reactions, but generously so. There is no reason to suspect that the unmeasured reactions are uniformly larger and that only the smallest appear in the literature. The best resolved limits are those bounding neutron contributions to a few tenths of a percent. It seems reasonable to conclude that in all cases examined in this work the (γ,γ') channels dominated by orders-of-magnitude.

The final results for the integrated cross-sections of the nuclides examined here are shown in Table IV, from which the normalized activations may be obtained with the information of Table I. The integrated cross-sections are given at the reference energy of 2.125 MeV but values at other energies may be obtained from the numbers in Table I. The limiting fraction of neutron activation present in the total activation is also displayed for isomers which could be produced by neutron capture in stable isotopes.

In addition to the materials listed, several other nuclei were irradiated. A sample was exposed which contained natural abundances of the nuclides, ^{107}Ag, whose isomer has a half-life of 44.2 sec and a fluorescence line at 93.2 keV, and ^{109}Ag, whose isomer has a 39.6 sec half-life and a photopeak at 88.0 keV. This sample was activated, but the resolution available with the NaI detector was not sufficient to separate the two contributions. The isomer $^{183}W^{m}$ was also successfully activated, but uncertainties in the transparency factor due to the nature of the sample prevented quantitative analysis in this case. Six

other isomeric nuclei, ^{207}Pb, ^{90}Zr, ^{177}Hf, ^{178}Hf, ^{176}Yb and ^{190}Os were irradiated but exhibited no measurable activation.

Table IV

Summary of experimental results. The quantity ΔJ is the change in spin between ground state and isomer. For both 4 and 6 MeV irradiations, the integrated cross-sections of a single gateway state at the reference energy of 2.125 MeV are given as $(\sigma\Gamma)$ and have been corrected for thermal and epithermal neutron contaminations. The term "units" is used for the sake of brevity to represent units of 10^{-29} cm^2-keV. Also given is the fraction of neutron contamination in the total activation, A_n/A_{Tot}, and the ratio of 6 MeV activation to 4 MeV activation, κ. The comment NA is used when no naturally abundant parent is available for (n,γ) reactions.

Nuclide	ΔJ	4 MeV $(\sigma\Gamma)$ [units]	4 MeV A_n/A_{Tot} [%]	6 MeV $(\sigma\Gamma)$ [units]	6 MeV A_n/A_{Tot} [%]	κ
^{167}Er	3	4225 ± 99	0.01	40611 ± 426	0.32	9.61
^{79}Br	3	607 ± 16	NA	2199 ± 27	NA	3.62
^{191}Ir	4	6995 ± 558	NA	42352 ± 1133	NA	6.05
^{197}Au	4	2383 ± 37	NA	15628 ± 75	NA	6.56
^{89}Y	4	8 ± 5	NA	307 ± 10	NA	38.38
^{77}Se	3	303 ± 4	0.03	7734 ± 38	0.76	25.52
^{179}Hf	4	8655 ± 112	0.04	29007 ± 128	6.41	3.35
^{137}Ba	4	304 ± 21	<0.01	2296 ± 27	0.07	7.55
^{199}Hg	6	234 ± 9	0.05	1686 ± 50	5.40	7.21
^{111}Cd	5	846 ± 11	<0.01	2992 ± 52	0.07	3.54
^{113}In	4	1182 ± 54	NA	5501 ± 208	NA	4.65
^{87}Sr	4	362 ± 12	<0.01	1027 ± 21	0.89	2.84
^{176}Lu	6	13212 ± 87	0.01	41502 ± 2680	1.51	3.14
^{115}In	4	1643 ± 15	NA	7936 ± 16	NA	4.83
^{180}Ta	8	16481 ± 6021	NA	41603 ± 772	NA	2.52
^{135}Ba	4	1152 ± 57	<0.01	7121 ± 134	0.39	6.18
^{195}Pt	4	2723 ± 150	<0.01	16521 ± 263	0.03	6.06
^{117}Sn	5	292 ± 43	<0.01	1040 ± 31	0.07	3.56
^{123}Te	5	3829 ± 672	<0.01	8038 ± 373	1.45	2.10

Conclusions

The values of the integrated cross-section shown in Table IV are unexpectedly large, in many cases two to three orders of magnitude larger than any previous results. The Breit-Wigner model indicates that these cross-sections correspond to remarkably large partial widths. Although these numbers are surprising, there are several considerations which inspire confidence in the results, not the least of which is the reproducibility of the findings under different experimental conditions. Perhaps the most compelling argument is seen in the result for the reaction $^{87}Sr(\gamma,\gamma')^{87}Sr^{m}$. As was previously mentioned, an early value was measured of 580 · 10^{-29} cm^2-keV for the integrated cross-section at 2.66 MeV. The current derived value for a hypothetical single gateway at 2.66 MeV taken from the 4 MeV irradiations is (613 ± 21) · 10^{-29} cm^2-keV. These two measurements are in good agreement when the amount of variability in early experiments is considered. The fact that the cross-section at the reference energy of 2.125 MeV obtained from the 6 MeV linac is 2.87 times larger than that from the 4 MeV exposures indicates that at least one other gateway has been accessed by photons with energies above about 3 MeV.

The example of ^{87}Sr demonstrates the utility of the single gateway assumption in discussing the results. Another important case is that of $^{123}Te^{m}$. Examination of Fig. 6 shows that the cross-section curves from the 4 and 6 MeV experiments become equal in the vicinity of 3 - 3.5 MeV. This would strongly imply that the reaction $^{123}Te(\gamma,\gamma')^{123}Te^{m}$ proceeds through a single mediating level located in this range, having an integrated cross-section of about 16500 · 10^{-29} cm^2 keV. If this is indeed true, $^{123}Te^{m}$ may form the cornerstone of the extension of the spectral calibration technique used in Refs. 11 and 12 to energies up to 6 MeV. The isomer $^{79}Br^{m}$ was instrumental in implementating this technique, as below 1.5 MeV it is photoactivated through only a single gateway at 761 keV with integrated cross-section of 6.2 · 10^{-29} cm^2-keV. It should be noted that no other nuclide in this study other than ^{123}Te exhibited such strong evidence for an actual single gateway state in the range of 1.5 - 6.0 MeV.

As stated earlier, the current values for the integrated cross-sections are orders of magnitude larger than those obtained in earlier experiments. It has been suggested that this is caused by non-resonant channels which open near the threshold for (γ,n) reactions. The state density is particularly high near this threshold and the earlier work,[15,16] conducted with sources having endpoint energies below 3 MeV, may not have accessed this process. However, this suggestion would not seem to be supported by the data. The ratios of activation with 6 MeV bremsstrahlung to that from 4 MeV bremsstrahlung, given in Table IV as κ, vary from 2.10 to 9.61 for all but two isomers. These ratios would not appear large enough to signify that a non-resonant process near the (γ,n) threshold was accessed by the few photons in the high energy tail of the bremsstrahlung spectrum. The exceptions to this behavior are ^{89}Y, with κ = 38.38, and ^{77}Se, having a ratio of 25.52. The magnitude of the cross-section determined for $^{89}Y^{m}$ from the 6 MeV irradiations, $(307 \pm 10) \cdot 10^{-29}$ cm^2-keV, would seem too small to be evidence for a non-resonant process which is directly related to the large state density above 4 MeV. However, for $^{77}Se^{m}$ it is possible that the larger cross-section, $(7734 \pm 38) \cdot 10^{-29}$ cm^2 keV, from the 6 MeV exposures does indeed point to this type of excitation mechanism. It is important to note that if this is the case, such a process is the exception rather than the rule in this energy range.

The pervasiveness found for the unexpectedly large values for the integrated cross-sections in this energy range suggests some type of core property varying slowly with increasing nuclear size. In such a case, however, there would seem to be the need for a mixing of several single particle states. The decay of the gateway level could then occur by several different cascades with comparable probabilities. The partial widths corresponding to these cross-sections are characteristic of relatively unhindered E1 transitions. Systematic studies[38] have shown that collective octupole oscillations of the nuclear core can unhinder E1 transitions, making very short lived states available for (γ,γ') reactions excited from ground states at energies between 1 and 2 MeV. The literature,[39] however, suggests that the branching for such a collective state would almost entirely favor the initial transition so that the product $b_a b_o$ would be severely diminished. This would largely offset the increased width Γ in expressions for the integrated cross-section. This expectation is supported by the early data of Refs. 15 and 16.

Since the density of states is elevated at energies of 1 to 2 MeV above the ground state, an alternate speculation is attractive. A strong collective oscillation of the core might serve to mix enough single particle states so that radiative branches to several different lower levels become comparable. In this case a very large integrated cross-section for photoexcitation of isomers through (γ,γ') reactions might be found to be only slightly dependent upon the detailed single particle assignments of neighboring nuclei. This would seem to be the case since the results of these experiments do not show a strong correlation with quantities such as ΔJ or its projection, ΔK.

The study of photoexcitation of isomeric nuclei through (γ,γ') reactions is obviously far from complete and detailed investigations which allow a final determination of the presence of resonant gateways are underway. These experiments employ several methods to modify the energy spectra of fixed endpoint sources and show great promise. Nevertheless, the lack of availability of a true variable endpoint source capable of producing sufficient photon fluences is still the largest single barrier to the measurement of the physical processes underlying these reactions.

References

1. B. Pontecorvo and A. Lazard, C. R. Acad. Sci. 208, 99 (1939).

2. G. B. Collins, B. Waldman, F. M. Stubblefield and M. Goldhaber, Phys. Rev. 55, 507 (1939).

3. K. Yoshihara, Zs. Nemeth, L. Lakosi, I. Pavlicsek and A. Veres, Phys. Rev. C 33, 728 (1986).

4. B. Harmatz, Nucl. Data Sheets 27, 453 (1979).

5. *Evaluated Nuclear Structure Data File* (Brookhaven National Laboratory, Upton, New York, 1986).

6. Y. Watanabe and T. Mukoyama, Bull. Inst. Chem. Res. 57, 72 (1979).

7. M. Krcmar, A. Ljubicic, K. Pisk, B. Logan and M. Vrtar, Phys. Rev. C 35, 1943 (1987).

8. I. Bikit, J. Slivka, I. V. Anicin, L. Marinkov, A. Rudic and W. D. Hamilton, Phys. Rev. C 35, 1943 (1987).

9. A. Ljubicic, K. Pisk and B. A. Logan, Phys. Rev. C 23, 2238 (1981).

10. N. Ikeda and K. Yoshihara, Radioisotopes 7, 11 (1958).

11. J. A. Anderson and C. B. Collins, Rev. Sci. Instrum. 58, 2157 (1987).

12. J. A. Anderson and C. B. Collins, Rev. Sci. Instrum. 59, 414 (1988).

13. C. B. Collins, J. A. Anderson, Y. Paiss, C. D. Eberhard, R. J. Peterson and W. L. Hodge, Phys. Rev. C 38, 1852 (1988).

14. J. A. Anderson, M. J. Byrd and C. B. Collins, Phys. Rev. C 38, 2838 (1988).

15. M. L. Wiedenbeck, Phys. Rev. 67, 92 (1945).

16. E. C. Booth and J. Brownson, Nucl. Phys. A98, 529 (1967).

17. C. B. Collins, C. D. Eberhard, J. W. Glesener and J. A. Anderson, Phys. Rev. C 37, 2267 (1988).

18. A. G. W. Cameron, in *Essays in Nuclear Astrophysics*, edited by C. A. Barnes, D. D. Clayton and D. N. Schramm (Cambridge Univ. Press, Cambridge, 1982), p. 23.

19. A. Richter and W. Ziegler, Private communication.

20. R. Mohan, C. Chui and L. Lidofsky, Med. Phys. 12, 595 (1985).

21. N. C. Ikoro, D. A. Johnson and P. P. Antich, Med. Phys. 14, 93 (1987).

22. *The EGS4 Code System*, Walter R. Nelson, Hideo Hirayama and David W. O. Rogers, SLAC Report 265 (Stanford Linear Accelerator Center, Stanford, Calif. 1985).

23. H. E. Johns and J. R. Cunningham, *Physics of Radiology*, Fourth Edition, (Charles C. Thomas, Springfield, Illinois, 1983), pp. 217 - 224, Appendix A - 3.B.

24. E. Browne and R. B. Firestone, *Table of Radioactive Isotopes*, edited by V. S. Shirley (Wiley, New York, 1986).

25. *Neutron Cross Sections: Volume II, Curves*, Third Edition, D. I. Garber and R. R. Kinsey, BNL 325 (National Neutron Cross Section Center, Brookhaven National Laboratory, Upton, New York, 1976).

26. A. Calamand, "Cross Sections for Fission Neutron Spectrum Induced Reactions" in *Handbook of Nuclear Activation Cross Sections*, International Atomic Energy Agency Technical Report Series No. 156 (IAEA, Vienna, 1974), pp. 273 - 324.

27. E. Ramstrom, Nucl. Phys. A315, 143 (1979).

28. H. A. Grench and H. O. Menlove, Phys. Rev. 165, 165 (1968).

29. H. C. Martin, B. C. Diven and R. F. Taschek, Phys. Rev. 93, 199 (1954).

30. C. P. Swann and F. R. Metzger, Phys. Rev. 100, 1329 (1955).

31. G. L. Sherwood, A. B. Smith and J. F. Whalen, Nucl. Sci. & Eng. 39, 67 (1970).

32. J. B. Guernsey and A. Wattenberg, Phys. Rev. 101, 1516 (1956).

33. K. Sakurai and I. Kondo, Nucl. Inst. and Meth. 187, 649 (1981).

34. *ASTM Standard Method for Determining Neutron Flux, Fluence and Spectra by Radioactivation Techniques*, Publication E 261-77 (American Society for Testing and Materials, Phyladelphia, 1987), and references cited there.

35. K. H. Beckurts and K. Wirtz, *Neutron Physics*, Trans. by L. Dresner (Springer-Verlag, New York, 1964).

36. *ASTM Standard Method for Determining Thermal Neutron Reaction and Fluence Rates by Radioactivation Techniques*, Publication E 262-86 (American Society for Testing and Materials, Philadelphia, 1987) and references cited there.

37. F. W. Walker, D. G. Miller and F. Feiner, Eds., *Chart of the Nuclides*, Thirteenth Edition (General Electric Company, San Jose, Calif. 1983).

38. A. de Schalit and H. Feshback, *Theoretical Nuclear Physics Vol. 1: Nuclear Structure* (Wiley, New York 1974).

39. C. F. Perdrisat, Rev. Mod. Phys. 38, 41 (1966).

LIMITS ON NEUTRON ACTIVATION INTERFERENCES IN PHOTOACTIVATION CROSS-SECTION MEASUREMENTS IN THE 1.5-6 MeV RANGE

by J. A. Anderson, C. D. Eberhard, J. J. Carroll, M. J. Byrd, and C. B. Collins
Center for Quantum Electronics, University of Texas at Dallas
and E. Scarbrough and P. P. Antich
University of Texas Southwestern Medical Center

Introduction

Recent measurements[1-4] have indicated that (γ,γ') cross sections at energies between 1.5 and 6 MeV may be three orders of magnitude or more greater than corresponding cross sections at lower energies. Since the high-energy photons used in these experiments can also produce neutrons through (γ,n) reactions, it is necessary to rule out contamination of the (γ,γ') cross section results by this incidental neutron field. This study establishes limits on the contributions of neutron reactions in previous experiments. Two basic approaches can be made toward this end: quantifying contributions from known neutron sources and making independent measurements of the neutron flux. Both approaches have been taken in this work and have been compared for mutual agreement. On the basis of this study, neutron-induced interferences are at least two to three orders of magnitude less than the observed isomeric activity due to photoexcitation.

Neutron Interference in Photoactivation Measurements

Two types of interfering neutron reactions can affect nuclear photoactivation studies on isomeric nuclei. The first is excitation of the isomer through (n,n') processes that populate the isomer either directly or through cascades from higher lying states. This, of course, requires neutrons with energies greater than the energy separation between the ground and isomeric states. All isomers can be excited

through the (n,n') process, which typically has a cross section on the order of several hundreds of millibarns. A summary of the isomers studied in references 1-4 is given in Table I. Note that $^{77}Se^{m}$, the lowest lying isomer which was excited from the ground state, requires a minimum neutron energy of 162 keV to initiate an (n,n') reaction. Measured integrated cross sections for isomeric photoactivation have been included in Table I. These values have been updated from previous reports to include additional trials and improved instrumental parameters. Because the earlier technique does not permit identification of a unique photoactivation gateway, a hypothetical single gateway at 2.125 MeV has been used to calculate the cross section values listed here. These values can be adjusted to other assumed gateway energies by using the spectrum of the bremsstrahlung source employed in these experiments[5,6] which is shown in Fig. 1. If the relative intensity of the source at 2.125 MeV is $\phi(2.125)$ and if the intensity at the desired energy E is $\phi(E)$, then the adjusted value for the cross section is given by

$$\sigma(E) = \sigma(2.125\ \text{MeV}) \times [\phi(2.125)/\phi(E)] \quad . \qquad (1)$$

Values for the ratio $\phi(2.125)/\phi(E)$ are tabulated in Table II.

Isomeric states can also be populated by neutron capture in the isotope having one less neutron than the isomer. This can occur through capture in either the resonance or thermal regions. For example, when neutron capture occurs in the 1.46 eV resonance of ^{115}In, there is an 79.5% probability of populating the 127 keV ($T_{1/2}$ = 54.1 min) isomer in ^{116}In. The remainder of the capture products populate[8] the ground state ($T_{1/2}$ = 14.1 s) of ^{116}In. In contrast, thermal neutron capture in ^{115}In can produce not only the $T_{1/2}$ = 54.1 min and $T_{1/2}$ = 14.1 s activities, but also $T_{1/2}$ = 2.16 s activity[9] from the 290 keV isomer in ^{116}In. This second, short-lived isomer decays to the 127 keV isomeric level through emission of a 162 keV photon.

Table I

Isomers studied in current investigations. Values for the nuclear parameters are taken from reference 7. Values for $\sigma\Gamma(2.125)$, the integrated cross section for an assumed gateway state at 2.125 MeV, are taken from the work references 1-4. In some cases, the cross sections have been upd from the previous values to reflect new data. When multiple trials of sample counts were available, the standard deviation of the mean has been given for the $\sigma\Gamma$ value.

Isomer	Ground State Abundance (%)	Energy (MeV)	Isomeric Halflife		J_g	J_i	$\sigma\Gamma(2.125)$ (10^{-29} cm^2-keV)
$^{77}Se^m$	7.6	0.162	17.45	s	1/2-	7/2+	7734 ± 38
$^{79}Br^m$	50.69	0.207	4.864	s	3/2-	9/2+	2200 ± 27
$^{87}Sr^m$	7.0	0.388	2.81	h	9/2+	1/2-	1037 ± 21
$^{89}Y^m$	100.0	0.909	16.06	s	1/2-	9/2+	306 ± 10
$^{111}Cd^m$	12.8	0.396	48.6	m	1/2+	11/2-	2994 ± 52
$^{113}In^m$	4.3	0.392	1.658	h	9/2+	1/2-	5501 ± 208
$^{115}In^m$	95.7	0.336	4.486	h	9/2+	1/2-	7938 ± 17
$^{117}Sn^m$	7.68	0.315	13.61	d	1/2+	11/2-	1040 ± 31
$^{123}Te^m$	0.91	0.247	119.7	d	1/2+	11/2-	8157 ± 372
$^{135}Ba^m$	6.59	0.268	28.7	h	3/2+	11/2-	7149 ± 134
$^{137}Ba^m$	11.74	0.662	2.5513	m	3/2+	11/2-	2297 ± 27
$^{167}Er^m$	22.95	0.208	2.28	s	7/2+	1/2-	40731 ± 426
$^{179}Hf^m$	13.63	0.375	18.68	s	9/2+	1/2-	30842 ± 117
$^{180}Ta^m$	0.00	0.032	1.2×10^{15}	y	1+	9-	41604 ± 772
$^{183}W^m$	14.3	0.309	5.15	s	1/2-	11/2+	3745 ± 1378
$^{191}Ir^m$	37.3	0.171	4.94	s	3/2+	11/2-	42354 ± 1133
$^{195}Pt^m$	33.8	0.259	4.02	d	1/2-	13/2+	16529 ± 264
$^{197}Au^m$	100.0	0.409	7.8	s	3/2+	11/2-	14503 ± 62
$^{199}Hg^m$	16.84	0.532	42.6	m	1/2-	13.5+	1783 ± 50

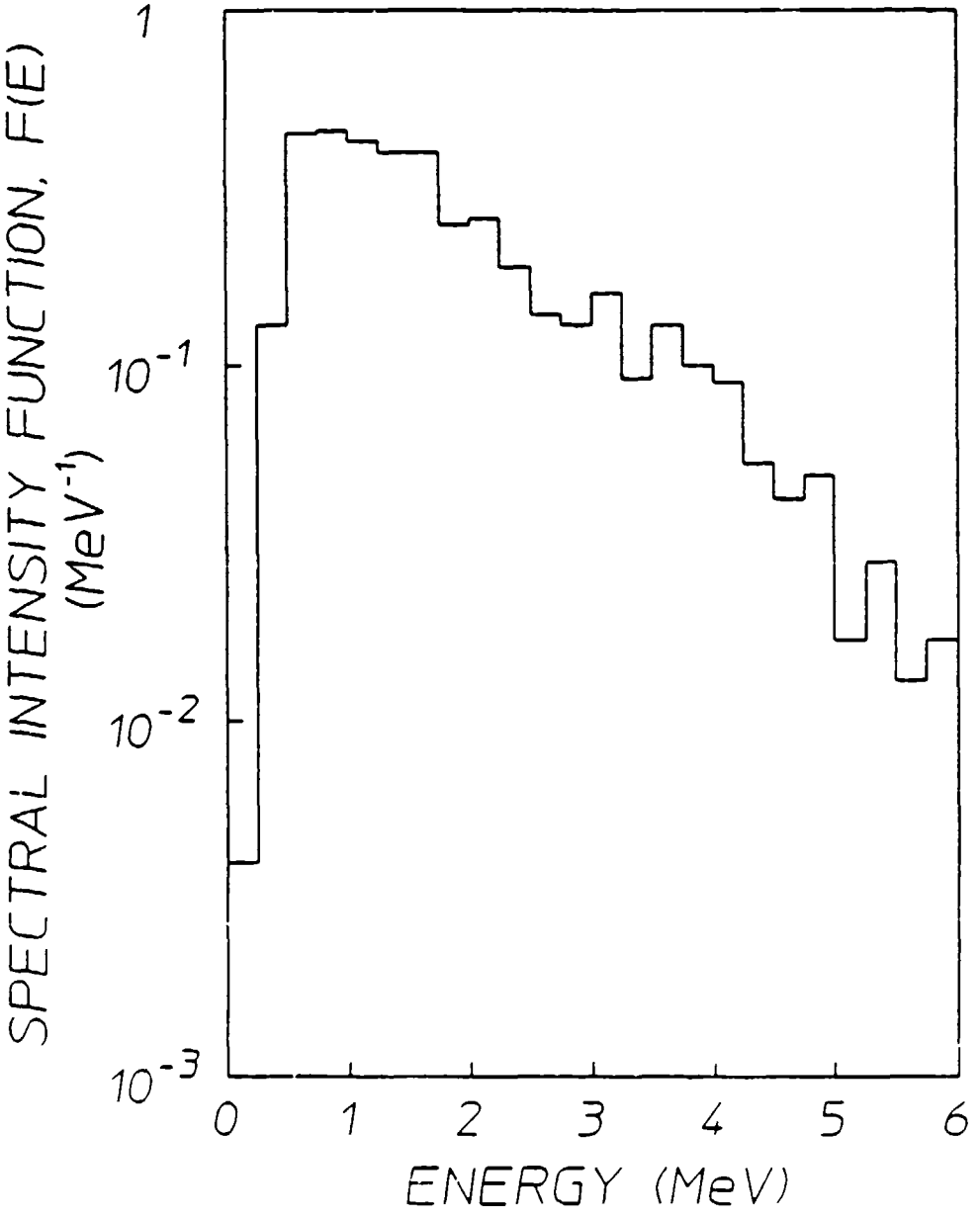

Figure 1: Relative spectral intensity for the bremsstrahlung used in the experiments of references 1-4. The values have been normalized so that the integral under the curve is unity.

Table II

Ratios of the photon intensities at energies E to that at 2.125 MeV for the spectrum shown in Fig. 1.

Energy [MeV]	$\phi(2.125)/\phi(E)$
0.125	0.015
0.375	0.500
0.625	1.731
0.875	1.769
1.125	1.654
1.375	1.538
1.625	1.538
1.875	0.962
2.125	1.000
2.375	0.731
2.625	0.538
2.875	0.500
3.125	0.615
3.375	0.354
3.625	0.500
3.875	0.385
4.125	0.346
4.375	0.204
4.625	0.162
4.875	0.188
5.125	0.065
5.375	0.108
5.625	0.050
5.875	0.065

Capture cross sections are quite small at high energy, but can be thousands of barns in the resonance and thermal energy regimes. However, in the experiments described in references 1-4, interference from this process requires that both the isotope undergoing capture and the ground state of the isomer be naturally occurring nuclides. A list of isomers from Table I satisfying this criterion and their appropriate capture cross sections is given in Table III.

Table III

Isomers susceptible to (n,γ) interferences and the isotopes which would produce them through neutron capture. The natural abundances of the capturing species are shown. Cross sections for total thermal capture (σ_T), thermal capture to the isomer ($\sigma_{T,I}$), total resonance capture (σ_R), and resonance capture to the isomer ($\sigma_{R,I}$) are listed.[9]

Isomer	Isotope	Natural Abundance[7] (%)	σ_T (b)	$\sigma_{T,I}$ (b)	σ_R (b)	$\sigma_{R,I}$ (b)
$^{77}Se^m$	^{76}Se	9.00	85	21.00	42	17
$^{87}Sr^m$	^{86}Sr	9.86	0.84	0.84	5	5
$^{111}Cd^m$	^{110}Cd	12.49	11.1	0.10	42	2
$^{117}Sn^m$	^{116}Sn	14.53	0.11	0.01	11.5	0.5
$^{123}Te^m$	^{122}Te	2.60	3		80	
$^{135}Ba^m$	^{134}Ba	2.42	2.16	0.16	20	
$^{137}Ba^m$	^{136}Ba	7.85	0.41	0.01	1.6	
$^{167}Er^m$	^{166}Er	33.60	20	15.00	100	
$^{179}Hf^m$	^{178}Hf	27.30	80	50.00	1900	
$^{183}W^m$	^{182}W	26.30	21		600	
$^{195}Pt^m$	^{194}Pt	32.90	1.2	0.10	4	
$^{199}Hg^m$	^{198}Hg	10.02	1.92	0.02	70	

Photoneutron Sources

The approximate threshold energy E_t for a (γ,n) reaction can be calculated from

$$E_t = \delta n + \delta(A-1,Z) - \delta(A,Z) \quad , \qquad (2)$$

where $\delta(A,Z)$ is the mass excess for the nuclide characterized by atomic number Z and mass number A, and δn is the mass excess for the neutron. The value calculated in this way does not include the correction necessitated by the recoil of the absorbing nucleus, but this is insignificant ($<<1\%$) in practice.

For monochromatic incident photons, neutrons produced by a (γ,n) reaction will also be nearly monochromatic because the momentum of the incident photon is very much less than that of the target nucleus. Part of the decay energy of the compound nucleus will be carried away by the recoil nucleus, resulting in the neutron energy, $E_n(\theta)$, being given[10] approximately by

$$E_n \approx \frac{M(E_\gamma - E_t)}{m + M} + \frac{E_\gamma[(2mM)(m + M)(E_\gamma - E_t)]^{1/2}}{(m + M)^2} \cos\theta \quad , \qquad (3)$$

where

θ = angle between the momentum vectors of the incident photon and emitted neutron,

E_γ = incident photon energy,

M = rest mass of recoil nucleus in energy units, and

m = rest mass of neutron in energy units = 938 MeV.

The second term, which contains the angular dependence of Eq. 3, is no more than 10% of the first term for the cases considered here and will be neglected in the following analysis.

Fast Neutron Contributions from Known Sources

The approximate neutron source spectrum and integrated neutron production rate for a given (γ,n) reaction can be calculated from the

incident photon spectrum using Eq. 3. Assuming that the target material is optically thin, the number N_n of neutrons produced in the range E_n to $E_n + \delta E_n$ from a sample of N_T target nuclei will be given by

$$N_n(E_n) = N_T \sigma(E_\gamma) \phi(E_\gamma)\, T\, \delta E_\gamma \quad , \tag{4}$$

where $\sigma(E_\gamma)$ is the (γ,n) cross section, $\phi(E_\gamma)$ is the spectral intensity in units of photons/cm^2-keV, T is the irradiation time, and $\delta E_n = \delta E_\gamma \times [M/(M + m)]$. The integrated production rate for all neutrons above a given energy E_n' is then simply

$$R_n(E_n') = N_n(E_n')/T = N_T \times \int_{E_{\gamma o}}^{E_{max}} \sigma(E_\gamma)\phi(E_\gamma) dE_\gamma \quad , \tag{5}$$

where $E_{\gamma o} = E_t + (1 + m/M)E_n'$.

High energy photons for the previous photoactivation studies were obtained from the bremsstrahlung output of a Varian CLINAC 1800 linac normally used for medical therapy. This source has been well characterized,[5,6] and its spectrum is shown in Fig. 1. The intensity reaches a maximum near 1 MeV and then drops by a factor of about thirty as it approaches its cut-off at 6 MeV. Therefore, the only neutron production mechanisms that are relevant are (γ,n) reactions with thresholds less than 6 MeV. A list of naturally occurring materials meeting this criterion is given in Table IV. Only these materials could serve as neutron sources in the experiments considered here. Several of them are rare and are not present in the linac construction or in its environment. The exceptions are ^{2}H, ^{9}Be, ^{13}C, and ^{17}O. Deuterium occurs as coolant water in the machine and as bound water in the concrete shielding of the irradiation cell. Beryllium is present in the beam exit window in the linac head. The other two possible contributors, ^{13}C and ^{17}O, occur in the atmosphere and in the shield walls of the linac cell. The cross sections[11] for ^{2}H and ^{9}Be are on the order of a few millibarns in the range between their reaction thresholds, near 2 MeV, and the maximum photon energy at 6 MeV. The thresholds for ^{13}C and ^{17}O are both above 4 MeV. The cross sections for these two nuclides are poorly known at such low energies, but may safely be assumed to be considerably less than a millibarn.[12,13]

Table IV

Naturally occurring materials with (γ,n) thresholds less than 6 MeV. The neutron energies, $E_{n,max}$, for neutrons ejected by 6 MeV photons were calculated neglecting the angular term in Eq. (3). The neutron binding energy, B_n, has been taken from reference 14.

Material	Natural Abundance (%)	B_n (keV)	$E_{n,max}$ (keV)
^{2}H	0.015	2224.6	1886.764
^{6}Li	7.5	5662	281.3626
^{9}Be	100	1665.1	3849.664
^{13}C	1.1	4946.5	971.7887
^{17}O	0.038	4142.5	1747.277
^{145}Nd	8.3	5760.4	237.9317
^{149}Sm	13.8	5846.2	152.7579
^{235}U	0.72	5307	690.0251

In the linac head itself, Be in the 0.025 cm thick beam window will be the dominant contributor to the neutron field. This is true because Be occurs monoisotopically as ^{9}Be, and has both a lower threshold energy (1.665 MeV vs 2.224 MeV) and a larger (γ,n) cross section averaged over the bremsstrahlung spectrum than ^{2}H. The beam window is located approximately 6 cm from the converter target and is illuminated over a diameter of about 3 cm. It comprises about 2.4×10^{22} ^{9}Be nuclei. Under equivalent irradiation conditions, almost 3 liters of normal water would be required to produce the same number of neutrons from the $^{2}H(\gamma,n)H$ reaction. This is far in excess of the several milliliters of water actually in the target cooling loop at any one time. Thus, for neutrons originating in the linac head, only those from the Be window are significant.

Under the assumptions that the photoneutrons are emitted isotropically from the Be foil[15] and that the foil dimensions are small compared to r, the source-sample distance, one obtains

$$\phi_n(E_n') = R_n(E_n')/(4\pi r^2) \qquad (6)$$

for $\phi_n(E_n')$, the intensity at the sample position of neutrons with $E_n \geq E_n'$. The results for a sample located at the position normally used for the work in references 1-4 are shown in Fig. 2. Note that the neutron intensity at the sample location due to this source is only 1000 n/(cm^2-s), about 7 orders of magnitude less than the corresponding integrated photon flux.

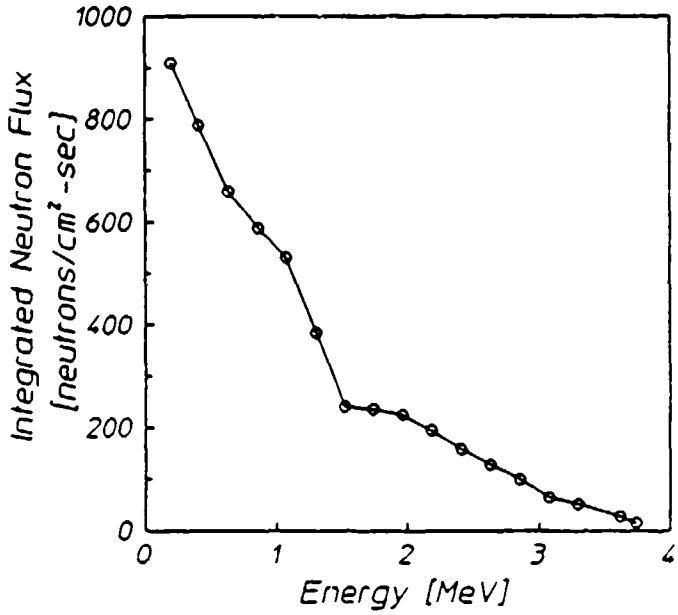

Figure 2: Calculated net neutron flux above the neutron energy E_n' at a distance of 65 cm from the bremsstrahlung source used for the work of references 1-4.

Neutron production due to (γ,n) reactions with ^2H, ^{13}C, and ^{17}O in the air is limited by the low density of the target nuclei, and, in the case of the last two materials, by small (γ,n) cross sections. If the x-ray output is assumed to pass through a conical volume with semi-angle $\theta_c = 8.75°$ --corresponding to the typical conditions of a field width of 20 cm at a sample distance of 65 cm -- then the volume of irradiated air

between the converter target and the floor is about 2.99×10^5 cm^3. The standard atmosphere[16] comprises 20.95% oxygen and 0.0314% carbon dioxide by volume. Using natural abundances of 0.038% and 1.1%, one obtains about 1.3×10^{21} atoms of ^{17}O and 2.8×10^{19} atoms of ^{13}C in the irradiated volume. A similar calculation for deuterium in the case of 100% relative humidity (T = 300 K) yields a result of 7.71×10^{19} ^2H atoms in the volume. Therefore, there are at least ten times more (γ,n) targets in the Be exit window on the linac than there are in the entire irradiated volume in the atmosphere. Moreover, most of the atmospheric targets occupy the bottom half of the cone, where the $1/r^2$ decrease in the photon beam intensity will have reduced the irradiation level by more than two orders of magnitude. As a result of these two conditions and the small cross sections for ^{17}O and ^{13}C, the atmospheric contribution to neutron production through the (γ,n) process is negligible compared to neutron production in the linac head itself.

The final possible source of neutrons in the linac environment is the concrete floor of the irradiation cell. Because an exact analysis of the concrete in place was not available, the typical composition[17,18] of concretes used in standard construction practice in this area was used to estimate the neutron production from this source. For a bulk density of 2.62 g/cm^3, atomic concentrations for the materials of interest were found to be as follows:

$$N(^2H) = 1.59 \times 10^{18} \text{ cm}^{-3} ,$$

$$N(^{13}C) = 8.16 \times 10^{19} \text{ cm}^{-3} , \text{ and}$$

$$N(^{17}O) = 1.91 \times 10^{19} \text{ cm}^{-3} .$$

Since the mass attenuation coefficient for a 6 MeV photon in concrete is about[19] 0.027 cm^2/g, the relaxation length for photons entering the floor slab is 14 cm. The neutrons created in the concrete obviously must escape the floor before being captured if they are to participate in (n,n') or (n,γ) processes in the sample, and therefore it is required that that contributing targets must lie within about 1 neutron migration length from the surface of the floor.[20] The neutron migration length is the sum, in quadrature, of the neutron slowing down length and the thermal diffusion length, and it can be considered to be the average straight line distance traveled between emission and thermalization of the neutron. For the composition model being used, the migration length for a 2 MeV neutron is 14 cm.[21] Thus, it is reasonable for the purposes of estimating the neutron flux from interac-

tions in the floor to assume that the neutrons originate in a cylindrical slab which is 15 cm thick and has the same diameter (d = 50.6 cm) as the beam envelope at floor level. Using Eq. 6, the estimated neutron flux at the sample position can be calculated for each of the species in the slab. The (γ,n) cross sections for ^{13}C and ^{17}O were assumed to have a constant value of 1 mb above the threshold energies; this represents a substantial overestimation. Measured cross sections[13] for ^{2}H were used. The results for the neutron fluxes produced by the different target nuclides are as follows:

$$\phi_n(^{2}H) = 0.08 \text{ n/cm}^2\text{-sec} \quad ,$$
$$\phi_n(^{13}C) = 0.8 \text{ n/cm}^2\text{-sec} \quad , \text{ and}$$
$$\phi_n(^{17}O) = 0.5 \text{ n/cm}^2\text{-sec} \quad .$$

As in the case of the atmospheric contributions, the contributions from the irradiation cell floor are insignificant compared to those from the Be beam window. Only the neutron flux produced by the Be window will be considered in the following analysis of contamination limits.

Contamination limits for the integrated cross sections listed in Table I could be directly determined from the integrated neutron flux shown in Fig. 2 and the appropriate cross sections for the (n,n') processes. Unfortunately, not all of the cross sections are known. To present the results of this study in a usable form even when the cross section data is not available, an alternate approach was chosen. For each of the materials in Table I, the (n,n') cross section that would be required to produce an arbitrary fraction f of the observed activation was calculated. A value of 100% was used for f in this work. The resulting cross sections have been compared with known (n,n') cross sections or other limiting cross sections, such as the total neutron cross section, when possible.

The (n,n') cross section necessary to produce the observed isomeric activation, $\sigma_{n,100\%}$, was obtained using the expression

$$\sigma_{n,100\%} = \frac{N_m}{N_T \, \phi_n(E_n') \, T} \quad . \qquad (7)$$

which follows from the assumption of negligible self-absorption effects. In this equation, N_m is the total number of isomers activated in the course of the irradiation, T is the time of the irradiation, and N_T is the number of ground state nuclei of the material of interest. A value

of $E_n' = 0$ was employed to evaluate Eq. 7, thus insuring that the minimum cross section value required would be obtained. Note that since the photoactivation cross section is obtained[1-4] from

$$(\sigma\Gamma)_\gamma = \frac{N_m}{N_T \phi_\gamma(E_\gamma) T} \quad , \tag{8}$$

the hypothetical neutron cross section required to produce the observed activation is related to the reported photon cross section by

$$\sigma_{n,100\%} = \frac{(\sigma\Gamma)_\gamma \phi_\gamma(E_\gamma)}{\phi_n(E_n')} \quad . \tag{9}$$

The (n,n') reaction cross sections which would have been necessary to produce the observed activations were calculated using Eq. (7) and have been tabulated as $\sigma_{n,100\%}$ in Table V. The actual total neutron cross sections and, where available, the non-elastic cross sections are also listed in Table V for the elements studied in references 1-4. Literature values for the true (n,n') cross sections for the selected isotopes are listed for those cases in which they are available. The actual (n,n') cross sections are on the order of several hundreds of millibarns or less. Some of the (n,n') cross sections listed in Table V are averages weighted against a fission spectrum. Although the fission spectrum is peaked at lower energies than the Be photoneutron spectrum whose integrated intensity is shown in Fig. 2, it still has significant intensity ($\approx 1/3\ I_{max}$) near 1 MeV, the point below which about half of the Be photoneutron intensity lies. Comparison of the (n,n') cross sections which would have been required account for the observed amounts of activation with the sizes of cross sections actually prevailing indicates that in all cases the neutron contamination is substantially less than 10%. The parameter Ω shown in Table V is the ratio of the best observed limiting cross section to $\sigma_{n,100\%}$. If the (n,n') cross section was available, then Ω was calculated using it; if not, then the non-elastic or total cross section was used. Thus, Ω always either equals or overestimates the ratio of the amount of true (n,n') induced activity to 100% of the observed activity in the photoactivation experiments, and thus it represents the fraction of fast neutron contamination expected in the photoactivation results. As can be seen from the table, Ω ranges from 0.0002 to about 0.06, corresponding to contamination limits for the photoexcitation results of between 0.02% and 6%. The maximum value of 6% occurs in the case of ^{79}Br, for which

only the total neutron cross section, rather than the smaller (n,n') cross section, was available. For the materials for which realistic values of the (n,n') cross section were available, the maximum fast neutron contribution to the observed isomeric activation is much less than 1%, based on an examination of all potential sources of fast neutrons in the experimental environment. This indicates that activation via the (n,n') reaction is not a significant process in the photoactivation studies being considered here.

Fast Neutron Flux Measurements

Measurement of such low neutron fluxes as the analysis above yielded at the sample position is difficult in the presence of an intense photon field. Although neutron counters based on the $^{10}B(n,\alpha)$ reaction or on the $^{3}He(n,p)$ reaction have some gamma-ray rejection capabilities, they are inadequate for the experimental situation encountered in this work. Boron counters are more robust than ^{3}He proportional tubes and can operate in gamma fields up to about 1000 R/hr, but the gamma field at the sample position in these experiments is about 60 times higher than this. Moreover, these counters are principally sensitive to thermal neutrons, and a moderator must be used to thermalize incident fast neutrons. Since the two most common and effective moderators are H and C, both potential sources of photoneutrons, there is also the possibility of creating a considerable perturbation in the neutron flux by introducing the detector.

Table V

Neutron cross sections required to produce 100% of the observed activation in previous photoexcitation studies[1-4]. Maximum values for the true total neutron cross section of the element of interest, σ_{el}, are shown for the energy range 0.1-6 MeV. When available, the non-elastic cross section for the element has been shown in parentheses following the total cross section. The most restrictive additional cross section, σ_{lim}, for the particular isotope or element is given with its type and E_{max}, the energy up to which it was determined. Cross section types are as follows: ie - inelastic in element; i - inelastic in isotope; n - non-elastic in isotope; fi - inelastic in isotope, average for fission spectrum. The factor Ω is the ratio of the most specific observed cross section to the cross section required for a 100% contamination effect, and thus represents an upper limit for contamination of the reported photoactivation cross section by neutron effects.

Isomer	$\sigma_{n,100\%}$ (b)	σ_{el} (b)	σ_{lim} (b)		Type	E_{max} (MeV)	Ω (%)
^{77}Se	490	8.3(2.4)	0.73	24	fi	-	0.15
^{79}Br	140	7.5					5.4
^{87}Sr	60	10	0.11	24	fi	-	0.18
^{89}Y	20	11.5	0.2	25	i	4.0	1.0
^{111}Cd	210	8	0.23	24	fi	-	0.11
^{113}In	320	6.3	0.047	26	i	1.0	2.0
^{115}In	430	6.3	0.38	27	i	5.3	0.088
^{117}Sn	70	6.8(2)					2.8
^{123}Te	530	6					1.1
^{135}Ba	420	7.3(2)					0.48
^{137}Ba	130	7.3(2)	0.66	28	i	3	0.51
^{167}Er	2700	9					0.33
^{179}Hf	1940	20	0.4	29	i	1.6	0.02
^{180}Ta	3016	8.5(2.9)	1.8	30	ie	1.8	0.06
^{183}W	140	9.3(2.4)	0.93	30	ie	1.7	0.66
^{191}Ir	2590	10.3					0.40
^{195}Pt	1350	10	0.68	30	ie	1.8	0.05
^{197}Au	95	10	1.3	30	i	5.3	0.14
^{199}Hg	120	10(2.6)	0.14	31	i	2.1	0.12

Another common approach to making fast neutron measurements is the use of neutron activation foils. Unfortunately, some of the most sensitive threshold reactions[33,34], are either (n,n') inelastic scattering reactions or (n,f) fission reactions, which can suffer from (γ,γ') or (γ,f) reaction interferences. However, other foils can be selected that have lower sensitivities but which are relatively free of photon induced interferences. A foil activation experiment was conducted to corroborate the results in the previous section and to verify that no significant neutron sources had been omitted from that analysis. Although the sensitivity of the experiment was inadequate to detect neutrons at the very low levels expected, it demonstrated that there were no unexpected neutron sources of significance in the environment.

Threshold detectors, commonly in the form of activation foils, have long been employed in the determination of neutron spectra. The techniques necessary for such measurements are well documented.[35] The practice is to expose a set of thin foils to the neutron flux in question. The materials of these foils are chosen to be sensitive to neutrons through a variety of reactions, such as (n,n'), (n,p), (n,2n) and (n,np). When the products of these reactions are sufficiently long-lived the activation due to each reaction can be easily measured. The number of activated nuclei produced, N_e, is given by

$$N_e = NT \int_0^\infty \sigma(E)\phi_n(E)dE \quad , \tag{10}$$

where N is the number of target nuclei, T is the irradiation time, $\sigma(E)$ is the reaction cross section, and $\phi_n(E)$ is the neutron spectral density at energy E. For a given material, each reaction occurs only when incident neutrons possess a kinetic energy greater than a particular threshold value. Thus each reaction can be thought of as sampling only the part of the total neutron spectrum which lies above the reaction's threshold, E_t. For this reason, Eq. 10 is often written as

$$N_e = NT\sigma_{eff} \int_{Et}^{\infty} \phi_n(E)dE \quad . \tag{11}$$

where σ_{eff} is the effective reaction cross section[35] and E_t is the threshold for the reaction. To determine a complete neutron spectrum, it is necessary to use a number of materials with different thresholds and to deconvolve the effects on all of these materials of neutrons in successively lower energy groups. The numerical procedure which used to accomplish this is called an unfolding.[36]

The experiment performed to determine the neutron flux present in the vicinity of the CLINAC 1800 operating in the 6 MeV photon mode employed Ti and Ni as foil materials. These were chosen for a variety of reasons. First, no naturally occurring isotopes of these elements possess isomeric states, so no (γ,γ') activation could occur. Next, (γ,n) and $(n,2n)$ reactions were not accessible since the threshold energy required for each exceeded that available from the linac. For those processes which were energetically possible, many had long lifetimes, important in our experiment. Finally, the thresholds of these reactions occurred at energies well suited for examining the energy range of interest. A summary of relevant properties of the reactions considered is given in Table VI.

Table VI

Accessible reaction properties for naturally abundant isotopes present in the chosen materials.[37]

Reaction	Daughter Halflife (d)	Signature Photon Energy (keV)
$^{46}Ti(n,p)^{46}Sc$	83.83	889.25
		1120.51
$^{47}Ti(n,p)^{47}Sc$	3.34	159.38
$^{58}Ni(n,p)^{58}Co$	70.92	810.79

The Ti and Ni foils were in the form of disks having radii of 2.54 cm and 0.65 cm and thicknesses of 0.005 cm and 0.025 cm. Two disks of each element were employed, with one disk of each encased in a Cd cover

to suppress activation due to thermal neutrons. All four disks were irradiated simultaneously at a distance of 65 cm from the bremsstrahlung converter and were oriented with their axes parallel to the direction of the beam. At the conclusion of a one hour irradiation, the samples were counted individually with a high purity germanium spectrometer system to determine the activation of the foils.

In general, for any peaks evident in the measured gamma-ray spectra which correspond to signature photons of reaction products, it is possible to determine the number of excited nuclei in each foil according to

$$N_e = \frac{C}{\eta f D A} \quad . \tag{12}$$

Here, C is the total number of counts observed within a peak, and η, f, D and A are the corrections for detector efficiency at the energy of interest, gamma ray intensity, finite duration of both irradiation and counting intervals, and self-absorption. This information can then be used in the unfolding process described above to make a determination of the neutron spectrum.

However, in the spectra obtained in this experiment no peaks were detectable above the level of the background, and a direct deconvolution could not be made. Instead, an upper bound for the neutron flux was determined by calculating the maximum number of counts in the signature photon peak which could have been hidden by the statistical variation of the background. The maximum number of excited nuclei was then found from Eq. 12. An upper bound for the neutron flux was then found with Eq. 11 for each reaction. These results are shown in Table VII, together with values of σ_o and E_t.

Table VII indicates that the (n,p) reaction on ^{58}Ni in the Cd covered foil provides the least upper bound for the neutron flux above 2.8 MeV, 8.72×10^3 n/cm^2-sec. Consideration of the spectrum of Fig. 2 implies the total neutron flux can be estimated from that above 2.8 MeV by increasing the value by a factor of 8. The neutron flux at the sample position must then be less than or equal to the maximum level of undetected neutrons in this experiment, 6.98×10^4 n/cm^2-sec. This is about two orders of magnitude greater than the limits obtained in the previous section; thus the experiment has inadequate sensitivity to

closely verify the preceding neutron source analysis, but does rule out the presence of significantly large sources which had not been included in that analysis. It should be noted that even the worst case neutron flux derived from this experiment would have only a small effect on the production of isomeric states through (n,n') reactions. For the case of $^{115}In^{m}$, a value for $(\sigma\Gamma)_\gamma$ at 2.125 MeV of 6700 x 10^{-29} cm^2-keV can be taken from Table I. With a photon flux incident on a sample at a distance of 65 cm of 5.7 x 10^6 photons/cm^2-keV-sec at 2.125 MeV and the maximum neutron flux taken from above, Eq. 9 indicates that an inelastic neutron scattering cross section of 5470 mb would be required to produce the observed amount of activation. Since the literature value from Table V is 380 mb, in this worst case scenario less than 10% of the observed isomeric activation could have been due to inelastic neutron processes.

Table VII

Calculated upper bounds for the neutron flux incident on the activation foils both with and without Cd covers. The values employed for σ_o and E_t[23] are also given.

Foil	Reaction Daughter	σ_o (mb)	E_t (MeV)	ϕ_n (10^3 n/cm^2-sec) wo/Cd	w/Cd
Ti	^{46}Sc	275	3.0	34.18	287.27
	^{47}Sc	21.4	2.2	29.91	107.48
Ni	^{58}Co	109	2.8	13.76	8.72

Thermal Neutron Measurements

Thermal and epithermal components of the neutron flux can be measured by a similar activation method. Samples in the form of foils are exposed to the unknown neutron flux, and the resulting activation

present in each foil is determined by standard counting techniques. Sample materials are chosen to be sensitive to (n,γ) neutron capture reactions in the thermal and resonance regions, rather than the (n,n') and (n,p) reactions considered previously. The foils are irradiated in pairs, one foil being fully exposed to the neutron flux, the other being enclosed in a cadmium cover. Because cadmium possesses a large thermal neutron capture cross section, a cover of about 0.076 cm thickness serves to remove almost all thermal neutrons from the flux seen by the shielded foil. Thus, the two foils will exhibit different activities, making it possible to calculate the separate thermal and epithermal neutron fluxes. This requires more than taking the simple difference of the foil activities, however, since a number of correction factors relating to neutron interactions in both the foils and the cadmium covers must be included. The approach used in this work is outlined in ASTM Standard E 262-86, "Standard Method for Determining Thermal Neutron Reaction and Fluence Rates by Radioactivation Techniques",[38] which includes numerous references to the literature. In this formalism, the thermal neutron flux, ϕ_{th}, is related to the saturated activities of the bare foil, A_s, and the cadmium covered foil, $A_{s,Cd}$, by

$$\phi_{th} = \frac{A_s}{g\sigma_o G_{th}} - \frac{A_{s,Cd}F_{Cd}}{g\sigma_o G_{th}}\left(1 + \frac{g\sigma_o}{G_{res}I_o} f_1 + \frac{\sigma_o w'}{G_{res}I_o}\right) , \qquad (13)$$

where the σ_o is the cross section for thermal neutron capture and I_o is the resonance integral. The two saturation activities A_x for the bare and cadmium covered foils are obtained directly from experiment as

$$A_x = \frac{N}{N_T T} , \qquad (14)$$

where N is the total number of excited nuclei produced, N_T is the number of target nuclei, and T is the irradiation period. Finally, the epithermal flux, ϕ_e, can be determined from

$$\phi e = \frac{A_{s,Cd}F_{Cd}}{I_o} . \qquad (15)$$

The factors g, w', f_1, G_{res}, G_{th}, and F_{Cd} occurring in Eq. 13 represent corrections[38] required by neutron interactions in both foils and in

the cadmium covers used with the epithermal neutron detector. Determination of thermal and epithermal neutron fluxes in the general case would require a detailed knowledge of the spectral distribution of the neutrons, which is typically not available. The problem is simplified if the detector material exhibits a cross section that varies inversely with its velocity, since then the reaction rates are proportional to the neutron density and are insensitive to the shape of the spectrum. In practice, the problem is formulated assuming that the detector material has a 1/v cross section behavior and the factor g appearing in Eq. 13 is introduced to correct for deviations from this ideal behavior. The correction factors f_1 and w' are required to account for epithermal activation of the detector material that occurs between the lower bound of the epithermal range (about 0.13 eV at room temperature) and the cutoff energy of the cadmium filter (about 0.5 eV). Again, a 1/v cross section is assumed for the purpose of calculating the principal correction f_1; deviations from 1/v behavior are corrected with factor w'. For both thermal and resonance reactions, if the foil is thick compared to the mean free path of a neutron, then corrections G_{th} and G_{res} for self-absorption of the neutrons must be made. Finally, in the case of indium the additional correction factor F_{Cd} is required.[39] The principal resonance in indium occurs at an energy of 1.44 eV, and the low energy wing of this resonance is affected by the presence of the cadmium cutoff filter. As a consequence, the observed number of counts from the epithermal detector must be increased by the factor F_{Cd} to account for the resulting reduction in activation.

An experiment was performed to investigate the thermal and epithermal flux produced in the environment of the CLINAC 1800 operating in the 6 MeV mode. Because more than one experimental objective was being pursued in this work, the linac was not operated in the vertical orientation used for the photoactivation measurements, but was operated horizontally. The principal difference resulting from this change in configuration was that the beam was stopped by the cell wall at a distance of about 4 m from the bremsstrahlung converter instead of the floor at a corresponding distance of 2.29 m. Two 0.0254 cm thick indium disks with diameters of 5.08 cm were simultaneously irradiated for 40 minutes at a distance of 100 cm from the photon source, with the axes of the disks parallel to the beam axis. The 0.076 cm thick cadmium cover used with the epithermal detector was formed of two 6.35 cm diameter disks stamped to create a recess for the indium sample to occupy. This

recess was slightly larger than that of the indium foil to insure its complete enclosure. After irradiation, the 54.15 minute half-life activity of the neutron capture product, $^{116}In^{m}$, was counted with a NaI(Tl) spectrometer system. Standard corrections for detection efficiency, finite transit and counting times, gamma ray intensity, and photon self-absorption were made.

The saturation activities for each foil were calculated from the ratio $N/N_T T$ and were found to be $A_s = (27.58 \pm .16) \times 10^{-20}$ min^{-1}, and $A_{s,Cd} = (11.82 \pm .13) \times 10^{-20}$ min^{-1}. Under the assumptions that the cadmium cutoff energy was 0.5 eV and that the neutrons were thermalized to room temperature (293.4 °K), f_1 was found to be 0.445 using the methods of ASTM E 262 . Values of σ_o, I_o, g, w', G_{th}, and G_{res} may also be found in that reference. Indium of the thickness used in this work presents an areal density of 177 mg/cm^2 to the neutron flux. Because relatively large cross sections are involved ($\sigma_o = 161$ b, $I_o = 2593$ b), these foils cannot be considered to be thin in comparison to the mean free path of a neutron, and the values of G_{th} and G_{res} differ substantially from 1. The cross section σ_o given above is for the activation of the 127 keV, 51.15 minute isomer $^{116}In^{m1}$ either directly or through the intermediate 290 keV, 2.18 s isomer $^{116}In^{m2}$. For the thickness of cadmium used in this experiment, the value of F_{Cd} was estimated[39] to be 1.15. The thermal and epithermal fluxes were then calculated to be

$$\phi_{th} = 12 \text{ n/cm}^2\text{-sec} \quad ,$$

and

$$\phi_e = 6 \text{ n/cm}^2\text{-sec} \quad .$$

It is possible to use these fluxes to estimate the interference effects that thermal and epithermal neutron activation might have on the photonuclear cross sections listed in Table I. The maximum activities that could be produced by the thermal flux, $A_{n,th}$, and by the epithermal flux, $A_{n,R}$, can be calculated with the cross sections listed in Table III by using

$$A_{n,T} = \sigma_{T,1}\phi_{th} \quad , \tag{16}$$

and

$$A_{n,R} = \sigma_{R,1}\phi_e \quad . \tag{17}$$

The activities A_p corresponding to the photoactivation cross sections in Table I can be obtained in a similar fashion for any arbitrary sample position from

$$A_p = \sigma(2.125)\phi(2.125) \quad , \qquad (18)$$

where $\sigma(2.125)$ is the single state cross section for a hypothetical state at 2.125 MeV and $\phi(2.125)$ is the spectral intensity at that energy in the sample position. Most of the photoactivation data previously obtained in this effort has been acquired with a sample distance of 65 cm ($\phi(2.125) = 5.7 \times 10^6$ photons/cm^2-sec).

Because the linac was used in a different geometrical configuration for the thermal and epithermal activation measurements than for the photoactivation studies, an estimated correction factor must be employed to obtain values for the neutron flux at the sample position in the correct geometry. This estimate was obtained from the consideration that the thermal neutrons must originate either in the cell floor or the linac head. Of these two possible sources, the cell floor is much more probable because of its substantial hydrogen content. Since the low energy neutrons are formed by what is effectively a secondary emission process, the functional dependence of the neutron flux on the position of the secondary source is analogous to the classic radar signal problem. If the sample and the photon source were at the same position, then the thermal neutron flux would depend on the inverse fourth power of the distance to the cell floor. Because the sample and the photon source are separated in this case, the flux should instead vary as the product of the inverse squares of the source-wall distance and the wall-sample distance. Using this approximation, the ratio of expected low energy neutron fluxes for the vertical and horizontal configurations described above was found to be about 10. It should be noted that for the less likely case in which the low energy neutrons originate in the linac head, the variation of the flux with sample position will depend only on the inverse square of the separation between the neutron source and the sample. Thus for the geometry existing in the experiments described here, the chosen correction factor will also form a comfortable upper bound in this second, less likely, case.

For the purpose of estimating potential neutron activation interferences with Eqs. 16 and 17, the neutron fluxes obtained by the foil activation experiment were multiplied by the geometrical factor dis-

cussed above. The expected isomeric activities due to neutron capture were then calculated for all materials from Table III for which the neutron activation cross sections for the isomeric states were available. These values and the experimentally observed activations calculated from Eq. 18 are tubulated in Table VII, which also lists Ω, the fraction of the observed activation that could be ascribed to neutron capture processes.

For those cases for which the neutron activation cross sections for populating isomeric states are not available, the upper bound for neutron contamination can be estimated by assuming that 100% of the neutron captures that occur lead to the isomeric state. The values for these upper limits were obtained by using the appropriate total neutron capture cross sections from Table III and are listed within parentheses in Table VIII. Note that even these cases, the degree of contamination of the photoactivation results is less than 6 percent except in the instance of $^{183}W^{m}$. For this nuclide, use of the total neutron capture cross section to estimate the interference with the (γ,γ') reaction indicates that the upper limit for contamination is about 30%. This may, of course, greatly overestimate the true amount of neutron interference since it represents only the limiting value.

In conclusion, for all cases in which the neutron cross sections are available, the neutron activation resulting from the measured thermal and epithermal neutron fluxes is less than 1% of the observed activation and thus represents a minimal contamination of the photoactivation measurement. Where the appropriate cross sections are not available and the total neutron capture cross section must be used to estimate the degree of neutron capture interference, only the case of $^{183}W^{m}$ presents the possiblity of significant contamination. Further resolution of the interference issue for this isotope will require additional information on the neutron activation cross section for ^{182}W associated with the production of the isomer $^{183}W^{m}$.

Table VIII

Interfering activities due to neutron capture processes calculated from measured thermal and epithermal neutron fluxes. Capture cross sections have been taken from Table III. The observed activites A_p attributed to photoactivation, the calculated thermal neutron activation $A_{n,T}$, and the calculated resonance neutron activation $A_{n,R}$ have been tabulated. The parameters Ω_T and Ω_R are the contamination limits, in percent, of the observed activation by neutron capture processes.

Isomer	A_p (sec^{-1})	$A_{n,T}$ (sec^{-1})	Ω_T (%)	$A_{n,R}$ (sec^{-1})	Ω_R (%)
$^{77}Se^m$	4.37×10^{-19}	2.5×10^{-21}	0.6	1.0×10^{-21}	0.2
$^{87}Sr^m$	5.62×10^{-20}	1.0×10^{-22}	0.2	3.0×10^{-22}	0.5
$^{111}Cd^m$	1.85×10^{-19}	1.2×10^{-23}	0.006	1.2×10^{-22}	0.06
$^{117}Sn^m$	5.88×10^{-20}	1.2×10^{-24}	0.002	3.0×10^{-23}	0.05
$^{123}Te^m$	4.54×10^{-19}	(3.6×10^{-22})	(0.08)	(4.8×10^{-21})	(1.0)
$^{135}Ba^m$	3.65×10^{-19}	1.9×10^{-23}	0.005	(1.2×10^{-21})	(0.3)
$^{137}Ba^m$	1.19×10^{-19}	1.2×10^{-24}	0.001	(9.6×10^{-23})	(0.08)
$^{167}Er^m$	2.42×10^{-18}	1.8×10^{-21}	0.07	(6.0×10^{-21})	(0.2)
$^{179}Hf^m$	1.74×10^{-18}	6.0×10^{-21}	0.3	(1.1×10^{-19})	(6.0)
$^{183}W^m$	1.24×10^{-19}	(2.5×10^{-21})	(2.0)	(3.6×10^{-20})	(29)
$^{195}Pt^m$	1.17×10^{-18}	1.2×10^{-23}	0.001	(2.4×10^{-22})	(0.02)
$^{199}Hg^m$	1.04×10^{-19}	2.4×10^{-24}	0.002	(4.2×10^{-21})	(4.0)

Conclusions

On the basis of this work, the previously reported results for photoactivation cross sections are substantially free of any contamination by neutron capture or neutron scattering processes. The upper limit for contamination by neutron induced activation of the observed isomeric states is less than 6% in all cases for which the appropriate neutron cross sections are available and significantly less than 1% in many instances. These conclusions are based on a consideration of both fast and slow neutron sources and the corresponding (n,n') and (n,γ) interference reactions. The major source of fast neutrons in the experimental environment when the CLINAC 1800 is operated in the 6 MeV bremsstrahlung mode is the beryllium beam window in the linac head. The total neutron flux at the sample position due to this source is about 1000 n/cm^2-sec. Direct measurement of the thermal and epithermal fluxes indicates that at the sample position there are about 120 n/cm^2-sec in the thermal range and 60 n/cm^2-sec in the epithermal region. Using these values for the incident neutron flux and appropriate literature values for the neutron cross sections for isomeric activation leads to the conclusion that neutron activation effects are about two orders of magnitude less than the observed photoactivation effects.

References

1. C. B. Collins, C. D. Eberhard, J. W. Glesener, and J. A. Anderson, Rapid Communications, Phys. Rev. C, 37, 2267 (1988).

2. C. B. Collins, J. M. Carroll, and J. A. Anderson, Center for Quantum Electronics Report #GRL/8702, University of Texas at Dallas, 1987 (unpublished), pp. 13-44.

3. C. B. Collins, J. A. Anderson, C. D. Eberhard, J. F. McCoy, J. J. Carroll, E. C. Scarbrough, and P. P. Antich, Center for Quantum Electronics Report #GRL/8703, University of Texas at Dallas, 1988 (unpublished), pp. 37-56.

4. J. A. Anderson, C. D. Eberhard, J. F. McCoy, K. N. Taylor, J. J. Carroll, M. J. Byrd, C. B. Collins, E. C. Scarbrough, and P. P. Antich, Center for Quantum Electronics Report #GRL/8704, University of Texas at Dallas, 1988 (unpublished), pp. 11-35.

5. R. Mohan, C. Chui, and L. Lidofsky, Med. Phys. 12, 595 (1985).

6. N. C. Ikoro, D. A. Johnson, and P. P. Antich, Med. Phys 14, 93 (1987).

7. J. K. Tuli, Nuclear Wallet Cards (National Nuclear Data Center, Brookhaven National Laboratory, 1985).

8. K. H. Beckurts and K. Wirtz Neutron Physics, Trans. by L. Dresner (Springer-Verlag, New York, 1964), p. 266.

9. F. W. Walker, D. G. Miller, and F. Feiner, Eds., Chart of the Nuclides, Thirteenth Edition (General Electric Company, San Jose, Calif. 1983).

10. G. F. Knoll, Radiation Detection and Measurement (John Wiley & Sons, New York, 1979) p. 34.

11. B. Bulow and B. Forkman, "Photonuclear Cross Sections," in Handbook on Nuclear Activation cross sections, International Atomic Energy Agency Technical Report Series No. 156 (IAEA, Vienna, 1974) pp 475-558.

12. K. Fukuda, Nucl. Phys. A156, 10 (1970).

13. J. W. Jury, B. L. Berman, D. D. Faul, P. Meyer, and J. G. Woodworth, Phys. Rev. C 21, 503 (1980).

14. J. A. Harvey and D. J. Hughes, "Neutrons,", in American Institute of Physics Handbook, Ed. D. E. Gray, (McGraw-Hill, New York, 1963).

15. T. Lauritsen and F. Ajzenberg-Selove, Nucl. Phys. 78, 1 (1966).

16. M. F. Harris, "Meteorological Information," in American Institute of Physics Handbook, ed. D. E. Gray (McGraw-Hill, New York, 1972).

17. Southwestern Laboratories of Dallas, TX, kindly provided us with information relating to typical concrete mixtures.

18. G. S. Brady, Materials Handbook, 9th Edition (McGraw-Hill, New York, 1963).

19. Radiological Health Handbook, U.S. Department of Health, Education, and Welfare (U.S. Government Printing Office, Washington, D.C., 1970).

20. S. Glasstone and A. Sesonske, Nuclear Reactor Engineering, Third Edition (Van Nostrand, New York, 1981), p. 180.

21. G. D. Myers, private communication. Calculated using SNUPAR V2A Schlumberger Nuclear Parameters Code written by D. C. McKeon and H. D. Scott, 1988.

22. S. Glasstone and A. Sesonske, Nuclear Reactor Engineering, Third Edition, (Van Nostrand, New York, 1981), p. 13.

23. D. I. Garber and R. R. Kinsey, Eds., Neutron Cross Sections, Volume II, Curves, National Neutron Cross Section Center, Brookhaven National Laboratory publication BNL 325, 1976.

24. A. Calamand, "Cross Sections for Fission Neutron Spectrum Induced Reactions" in Handbook on Nuclear Activation cross sections, International Atomic Energy Agency Technical Report Series No. 156 (IAEA, Vienna, 1974) pp 273-324.

25. E. Ramstrm, Nucl. Phys. A215, 143 (1979).

26. H. A. Grench and H. O. Menlove, Phys. Rev. 165, 1638 (1968).

27. H. C. Martin, B. C. Diven, and R. F. Taschek, Phys. Rev. 93, 199 (1954).

28. C. P. Swann and F. R. Metzger, Phys., Rev. 100, 1329 (1955).

29. G. L. Sherwood, A. B. Smith, and J. F. Whalen, Nucl. Sci. & Eng. 39, 67 (1970).

30. J. B Guernsey and A. Wattenberg, Phys. Rev. 101, 1516 (1956).

31. K. Sakurai and I. Kondo, Nucl. Inst. and Meth. 187, 649 (1981).

32. G. F. Knoll, Radiation Detection and Measurement (John Wiley & Sons, New York, 1979), p. 529.

33. Activation Foil Manual, distributed by Reactor Experiments Inc., 1965, and the references cited there.

34. ASTM Standard Method for Determining Neutron Flux, Fluence, and Spectra by Radioactivation Techniques, Publication E 261-77, (American Society for Testing and Materials, Philadelphia, 1987) and references cited there.

35. K. H. Beckurts and K. Wirtz, Neutron Physics, Trans. by L. Dresner (Springer-Verlag, New York, 1964), p. 286.

36. Foil Activation Data Unfolding Code (FATDUD), from the RSIC Computer Code Collection, Radiation Shielding Information Center, Oak Ridge National Laboratory.

37. E. Browne & R. B. Firestone, Table of Radioactive Isotopes, Ed. by V. S. Shirley (John Wiley & Sons, New York, 1986).

38. ASTM Standard Method for Determining Thermal Neutron Reaction and Fluence Rates by Radioactivation Techniques, Publication E 262-86, (American Society for Testing and Materials, Philadelphia, 1987) and references cited there.

39. C. W. Tittle, Nucleonics 8, 6 (1951).